JOURNAL OF THE AERONAUTICAL SCIENCES

VOLUME 9 AUGUST, 1942 NUMBER 10

The Correction of Engine Output to Standard Conditions

DONALD S. HERSEY*

United Aircraft Corporation

SUMMARY

In order to provide a common basis for the comparison of high-performance supercharged aircraft engines, formulas are proposed for correcting the measured output to standard atmospheric conditions.

An investigation of power-correction formulas is needed because the formulas generally used were developed for naturally aspirated engines and have been found inaccurate when applied to supercharged-engine test data.

In the development of the proposed correction formulas, the theoretic effects of atmospheric changes on the performance of an engine's induction system units are discussed and applied in a general basic correction formula. These effects pertaining to each induction system unit are checked by comparing the unit formula with test data obtained on a specific engine.

Two engine-output correction formulas, covering both full-throttle and part-throttle operation of single-stage supercharged engines, are then evolved. The accuracy of these formulas is determined by comparison of calculated engine performance with flight test data taken under various atmospheric conditions. A similar check of the correction formulas generally used is also made.

A comparison of the old and new full-throttle formulas indicates that former correction errors of as much as 10 per cent may now be reduced to approximately $1^1/_2$ per cent. Comparison of the part-throttle correction formulas shows that the accuracy of the rational formula is slightly inferior to that of the generally used formula.

Correction formulas for two-stage supercharged engines of the gear-driven and turbo-driven variety are finally proposed for consideration, but no flight test proof of these latter formulas is presented.

The conclusions reached as a result of the correction formula investigations are:

1. The formula derived for use in correcting the full-throttle output of single-stage supercharged engines is basically more sound and considerably more accurate than the generally used full-throttle power correction formula.

2. The rational formula derived for use in correcting the part-throttle output of single-stage supercharged engines shows no superiority over the empirical part-throttle correction formula now in general use.

3. The correction formulas proposed for use in connection with engines equipped with two-stage gear-driven and turbo-driven superchargers should give reasonable accuracy, although some experience must be gained in the use of these formulas before they are finally adopted.

Presented at the Power Plants Session, Tenth Annual Meeting, I.Ae.S., New York, January 28, 1942.

* Project Engineer, Pratt & Whitney Aircraft Division.

LIST OF SYMBOLS

C	= supercharger density parameter = $\left[\frac{V^2}{6088T_b}+1\right]^{2.53}$
C_k	= constant representing the ratio of the pressure head of cooling air on passing through the intercooler, to the airplane pressure head, q. $C_k = \sqrt{\frac{5.2(p_k - p_b)}{^1/_2\,(\delta_k/32.17)\,V_c^2}}$
D (cu.in.)	= engine displacement (swept volume)
e	= intercooler effectiveness = $e = (T_{d_1} - T_d)/(T_{d_1} - T_k)$
g (ft. per sec.^{2})	= acceleration due to gravity
i	= subscript to denote "observed" conditions
k	= ratio of specific heat values of air = $C_p/C_v = 1.3947$
K_c	= equivalent orifice constant of carburetor at full-throttle setting
K_k	= equivalent orifice constant representing the cooling air restriction losses through the intercooler and its cooling air ducts
K_u	= equivalent orifice constant representing the engine air restriction losses through the intercooler and its engine air ducts
N (r.p.m.)	= engine crankshaft rotative speed
n (r.p.m.)	= turbosupercharger impeller speed
p_a (in. Hg)	= absolute pressure in the atmosphere
p_b (in. Hg)	= absolute pressure at the main-stage supercharger entrance
p_{b_1} (in. Hg)	= absolute pressure at the auxiliary-stage supercharger entrance
p_c (in. Hg)	= absolute pressure at the carburetor entrance
p_d (in. Hg)	= absolute pressure at the main stage supercharger discharge annulus

p_{d_1} (in. Hg) = absolute pressure at the auxiliary stage supercharger discharge annulus
p_e (in. Hg) = absolute exhaust back pressure
p_h (in. Hg) = absolute pressure at the cooling air exit face of the intercooler
p_k (in. Hg) = absolute pressure at the cooling air entrance face of the intercooler
p_r (in. Hg) = absolute pressure at the exit of the ram scoop
Q_u (cu.ft. per sec.) = volumetric flow rate of engine air through the intercooler
Q_k (cu.ft. per sec.) = volumetric flow rate of cooling air through the intercooler
R_a (ft.lbs. per lb. per °F.) = gas constant for air (53.35)
R_i (ft.lbs. per lb. per °F.) = gas constant for intake charge mixture
s = subscript to denote "standard" conditions
S_k (sq.ft.) = intercooler cooling air face area
S_u (sq.ft.) = intercooler engine air face area
T_a (°R.)t_e (°F.) = absolute temperature of the atmosphere
T_b (°R.) = absolute temperature at the main-stage supercharger entrance
T_{b_1} (°R.) = absolute temperature at the auxiliary-stage supercharger entrance
T_c (°R.) = absolute temperature at the carburetor entrance
T_d (°R.) = absolute temperature at the main-stage supercharger discharge annulus
T_{d_1} (°R.) = absolute temperature at the auxiliary-stage supercharger discharge annulus
T_k (°R.) = absolute temperature of the cooling air to the intercooler
T_r (°R.) = absolute temperature at the ram-scoop exit
V (ft. per sec.) = main-stage impeller tip velocity
V_1 (ft. per sec.) = auxiliary-stage impeller tip velocity
V_a (ft. per sec.) = true airplane velocity
V_c (ft. per sec.) = velocity of the inducted air at the carburetor
V_r (ft. per sec.) = velocity of the inducted air at the ram-scoop exit
V_u (ft. per sec.) = velocity of the inducted air at the intercooler engine air face
W_d (lbs. per hour) = mass flow of dry air inducted by engine
W_f (lbs. per hour) = flow of fuel to the engine
W_k (lbs. per sec.) = mass flow of cooling air through the intercooler
W_t (lbs. per hour) = total flow of fluid inducted by engine
W_u (lbs. per sec.) = mass flow of engine air through the intercooler
W_w (lbs. per hour) = mass flow of atmospheric water vapor into the engine
Y = main stage supercharger pressure parameter = $[(p_d/p_b)^{0.283} - 1]$
Y_1 = auxiliary stage supercharger pressure parameter = $[(p_{d_1}/p_{b_1})^{0.283} - 1]$
Y_r = ram scoop pressure parameter = $[(p_r/p_a)^{0.283} - 1]$
b.hp. (hp.) = engine brake horsepower output
f.hp. (hp.) = engine motoring friction horsepower
i.hp. (hp.) = engine indicated horsepower (b.hp. + f.hp.)
i.s.a.c. (lbs. per i.hp.-hour) = indicated specific air consumption
δ_b (lbs. per cu.ft.) = density of inducted charge at entrance of main-stage impeller
δ_d (lbs. per cu.ft.) = density of inducted charge at discharge annulus of main-stage supercharger
δ_k (lbs. per cu.ft.) = density of cooling air entering the intercooler cooling air face
δ_u (lbs. per cu.ft.) = density of inducted charge entering the intercooler engine air face
η = main-stage supercharger pressure coefficient
η_1 = auxiliary-stage supercharger pressure coefficient
η_r = ram-scoop pressure coefficient
η_v = engine cylinder volumetric efficiency based on the density at the main-stage supercharger discharge annulus
θ = symbol representing the ratio: $(\delta_d/\delta_b)_{actual}/(\delta_d/\delta_b)_{adiabatic}$
ϕ = main stage supercharger temperature coefficient
η' = mechanical efficiency of engine at sea level
λ = ratio of mechanical friction to total friction horsepower at sea level
ϕ_1 = auxiliary-stage temperature coefficient

Introduction

As a result of flight-test and test-stand investigations made some years ago on naturally aspirated engines,[1, 2] the following formulas were derived for the correction of engine output to standard atmospheric conditions. At full throttle

$$\text{b.hp.}_s = \text{b.hp.}_i \left[\frac{p_{c_s}}{p_{c_i}} \sqrt{\frac{T_{c_i}}{T_{c_s}}} \left(1 + \frac{\lambda - \lambda\eta'}{\eta'} \right) - \left(\frac{\lambda - \lambda\eta'}{\eta'} \right) \right] \quad (1)$$

Because the ratio $(\lambda - \lambda\eta'/\eta')$ had relatively minor importance at full-throttle conditions, it soon was almost universally dropped. Hence, the full-throttle formula now in general use is:

$$\text{b.hp.}_s = \text{b.hp.}_i \left[(p_{c_s}/p_{c_i}) \sqrt{T_{c_i}/T_{c_s}} \right] \quad (2)$$

At part throttle, constant manifold pressure is assumed, and the term p_{c_s}/p_{c_i} does not apply. With constant pressure in the induction system, the generally used part-throttle correction formula becomes:

$$\text{b.hp.}_s = \text{b.hp.}_i \sqrt{T_{c_i}/T_{c_s}} \quad (3)$$

Ever since the engine torque indicator has come into use in determining power output in flight, numerous cases have arisen in which the application of the full-throttle output-correction formula, Eq. (2), has definitely given inaccurate corrected-output values.

Because of this situation, an extensive investigation was conducted to discover the causes of power-correction-formula inaccuracies. In this investigation both theoretic and practical studies were made and com-

pared. It is the purpose of this paper to present the results of these investigations.

General Analysis and Development of Theoretic Power-Correction Formulas

In correcting engine output to standard conditions, two different points of view may be taken: The engine manufacturer generally wants to know what corrected output his engine will deliver if standard atmospheric pressure and temperature values are substituted for the observed values that existed at the induction-system entrance when the output was measured. This correction of observed output to standard conditions provides a common basis on which engines of different design or manufacture can be compared.

The airplane manufacturer is not especially interested in comparing engines. He wishes to know how his airplane will perform in standard atmosphere but can seldom test it when the free air temperature, pressure and humidity are at arbitrary N.A.C.A. standard values. Therefore he must calculate the effect on airplane performance of correcting the engine output to correspond to standard atmospheric values at the airplane's air scoop entrance. This permits him to evaluate his airplane's performance with respect to the performance of other airplanes when flying in identical atmospheres.

Both points of view will be considered in the development of the following engine-output correction formulas.

Basis of Engine-Output Correction Formulas

The fundamental basis of Otto-cycle engine-output relations is that which expresses the output as a function of the air consumption. When the engine is operated at fixed values of fuel-air-mixture ratio and spark setting, the engine power is found to vary in a linear relation to the dry mass airflow. That is:

$$\text{i.hp.} = W_d/\text{i.s.a.c.} \tag{4}$$

In this relation the indicated specific air consumption is a constant that depends on the mixture-ratio, spark-advance setting and the combustion efficiency of the fuel mixture. As spark-setting and fuel-heating values are normally constant, it is primarily a function of the fuel-air-mixture ratio of the intake charge, although this function may be modified slightly by large changes of engine speed.

The mass flow rate of fluid inducted by the engine cylinders is the sum of the flow rates of dry air, fuel and the water-vapor content of the inducted air. This may be expressed by the relation

$$W_t = W_d\left[1 + \frac{W_f}{W_d}\right]\left[1 + \frac{W_w}{W_d}\right] \text{(approx.)} \tag{5}$$

At the entrance of the engine intake manifold, the total fluid induction rate may be expressed by the following equation:

$$\dot{W}_t = (D/1{,}728)(60N/2)\eta_v\delta_d \tag{6}$$

Eqs. (6), (5) and (4) may be combined, and the sum of the brake and friction horsepower may be substituted for the indicated horsepower to give the equation:

$$\text{b.hp.} = \frac{0.01736DN\eta_v\delta_d}{\text{i.s.a.c.}\left[1 + \frac{W_f}{W_d}\right]\left[1 + \frac{W_w}{W_d}\right]} - \text{f.hp.} \tag{7}$$

If the subscripts i and s are now used to denote observed and standard conditions of engine operation, respectively, the basic relation of standard to observed brake output is:

$$\text{b.hp.}_s = [\text{b.hp.}_i + \text{f.hp.}_i] \times \left[\frac{N_s\eta_{v_s}\delta_{d_s}\text{i.s.a.c.}_i\left(1 + \frac{W_f}{W_d}\right)_i\left(1 + \frac{W_w}{W_d}\right)_i}{N_i\eta_{v_i}\delta_{d_i}\text{i.s.a.c.}_s\left(1 + \frac{W_f}{W_d}\right)_s\left(1 + \frac{W_w}{W_d}\right)_s}\right] - \text{f.hp.}_s \tag{8}$$

This is the formula on which the subsequently described methods of correcting engine output to standard conditions are based. It is a general equation that is satisfactory for use with any four-stroke, Otto-cycle engine.

In the development of correction formulas the problem is to evaluate the different factors of Eq. (8) as functions of the atmospheric pressure, temperature and humidity so that the effects of atmospheric changes on engine output may be determined.

Development of Correction Factors for an Engine with a Single-Stage Supercharger and Supercharger-Entrance Carburetor

For a conventional carbureted engine equipped with a single-stage supercharger, the engine-air induction and exhaust-gas disposal system is similar to that shown in Fig. 1. In the airplane installation, a forward-facing intake air scoop is generally employed to provide "ram," as a result of the forward velocity of the airplane. A test-stand installation is more likely to provide an air-measuring and pressure-and-temperature regulating system than a forward-facing air scoop.

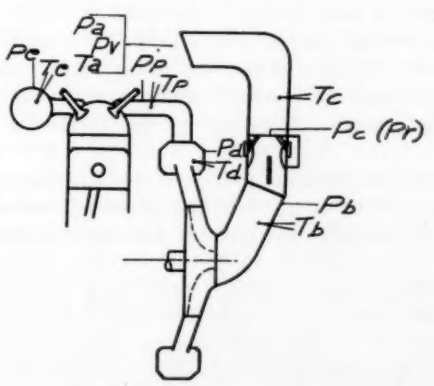

FIG. 1. Typical single-stage engine induction system diagram.

The basic difference between correction formulas for test-stand and airplane use lies in the fact that test-stand power corrections are made on the basis of the inducted air conditions at the entrance flange of the carburetor, whereas the airplane power corrections are made on the basis of the free-air conditions at the entrance of the forward-facing scoop.

Full-Throttle Conditions

At full throttle the inducted air undergoes numerous temperature and pressure changes before it reaches the entrance of the intake manifold. These changes are due to velocity variations in the air stream which are brought about by the supercharger and ram scoop, as well as by losses due to the carburetor chokes and throttles, the duct walls and elbows, and by the vaporization of the fuel as it mixes with the air stream.

Changes in state of the inducted air due to these different factors will now be considered.

Scoop Effects on the Inducted Air

The forward-facing airplane scoop produces both a pressure and a temperature rise which are functions of the scoop efficiency and the airplane speed, according to the relations:[3]

$$p_c = p_r = p_a\left[1 + \left(\eta_r \frac{k-1}{k}\frac{V_a^2 - V_r^2}{2gR_aT_a}\right)\right]^{k/k-1} = p_a\left(1 + \eta_r \frac{V_a^2 - V_r^2}{12{,}176T_a}\right)^{3.53} \quad (9)$$

$$T_c = T_r = T_a\left[1 + \left(\frac{k-1}{k}\right)\left(\frac{V_a^2 - V_r^2}{2gR_aT_a}\right)\right] = T_a\left(1 + \frac{V_a^2 - V_r^2}{12{,}176T_a}\right) \quad (10)$$

Because the scoop efficiency is practically impossible to determine, except under actual test conditions, not only the relation of p_c to p_a but also the ratio T_c to T_a must be measured during the flight test. Reasonably accurate means of estimating the carburetor-entrance pressure and temperature for standard conditions of the atmosphere are then available. For these estimations the scoop efficiency is assumed to remain constant despite the small variations in atmospheric conditions and airplane speed accompanying the correction process.

For the airplane installation of a single-stage engine the relations of standard to observed carburetor-entrance pressures and temperatures are as follows:

$$\frac{p_{c_s}}{p_{c_i}} = \frac{p_{r_s}}{p_{r_i}} = \frac{p_{a_s}}{p_{r_i}}\left[1 + (Y_{r_i})\left(\frac{V_{a_s}^2 - V_{r_s}^2}{V_{a_i}^2 - V_{r_i}^2}\right)\left(\frac{T_{a_i}}{T_{a_s}}\right)\right]^{3.53} \quad (11)$$

$$\frac{T_{c_s}}{T_{c_i}} = \frac{T_{r_s}}{T_{r_i}} = \frac{(T_{r_i} - T_{a_i})\left(\frac{V_{a_s}^2 - V_{a_s}^2}{V_{a_i}^2 - V_{r_i}^2}\right) + T_{a_s}}{T_{r_i}} \quad (12)$$

These ram-scoop relations are not used in test-stand power corrections as the standard carburetor-entrance pressure and temperature are assumed to be equal to the standard free-air pressure and temperature values as determined from *N.A.C.A. Report No. 218.*[4]

Carburetor Effects on the Inducted Air

As the inducted air passes from the entrance scoop or duct on through the carburetor, there is a pressure loss created by the carburetor chokes and throttles. At part-throttle setting this loss is of large magnitude and, furthermore, is unpredictable. Fortunately, calculations of the pressure drop through the carburetor need to be made only at full-throttle setting. A relation of the form

$$p_c - p_b = K_c p_c V_c^2/T_c \quad (13)$$

will evaluate this full-throttle pressure drop. The ratio of standard to observed impeller-entrance pressure may be expressed in terms relative to conditions at the carburetor entrance as follows:

$$\frac{p_{b_s}}{p_{b_i}} = \left(\frac{p_{c_s}}{p_{c_i}}\right)\left(\frac{1 - K_c V_{c_s}^2/T_{c_s}}{1 - K_c V_{c_i}^2/T_{c_i}}\right) \quad (14)$$

The temperature drop through the carburetor, due to fuel vaporization, is found to be dependent mainly upon the initial temperature of the entering air and the fuel-air ratio, regardless of throttle setting. Experimental data collected from several sources indicate that the drop in carburetor-air temperature due to vaporization may be calculated with sufficient accuracy by either of the empirical relations:

$$T_b = 21.4\sqrt{T_c} \quad (15)$$

or

$$T_b = 0.521(t_c + 873) \quad (16)$$

Other data (Fig. 2) indicate that changes in fuel-air-mixture ratio affect these calculated temperatures to only a minor degree and that further temperature drop

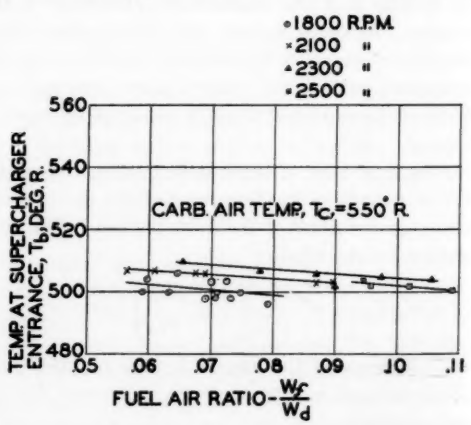

FIG. 2. Effect of fuel-air ratio on the primary-stage impeller-entrance temperature.

calculations involving the fuel-air ratio are unwarranted. Hence, the ratio of observed to standard impeller-entrance temperature becomes:

$$T_{b_i}/T_{b_s} = \sqrt{T_{c_i}/T_{c_s}} = (t_{c_i} + 873)/(t_{c_s} + 873) \quad (17)$$

Supercharger Effects on the Inducted Air

On passing through the supercharger the inducted mixture of fuel and air is subjected to an appreciable pressure, temperature and density rise. When only air is the fluid worked upon, the accepted supercharger relations that express the pressure and temperature ratios as functions of the impeller tip speed and impeller-entrance temperature are:

$$p_d/p_b = [(\eta V^2/6{,}088T_b) + 1]^{3.53} \quad (18)$$

and

$$T_d/T_b = [(\eta V^2/\phi\ 6{,}088T_b) + 1] \quad (19)$$

Should perfect adiabatic compression be assumed, the pressure and temperature coefficients are equal to unity, by definition. Therefore, the adiabatic supercharger outlet-to-inlet density ratio is found by division of Eq. (18) by Eq. (19) as follows:

$$\left(\frac{\delta_d}{\delta_b}\right)_{adiabatic} = \left(\frac{p_d}{p_b}\right)\left(\frac{T_b}{T_d}\right)_{adiabatic} = \left(\frac{V^2}{6{,}088T_b} + 1\right)^{2.53} \quad (20)$$

Let the measured density rise ratio, divided by the calculated adiabatic density rise ratio, be a parameter represented by θ. Then

$$\theta = \frac{(\delta_d/\delta_b)_{actual}}{(\delta_d/\delta_b)_{adiabatic}} = \frac{(\delta_d/\delta_b)_{actual}}{\left[\frac{V^2}{6{,}088\ T_b} + 1\right]^{2.53}} = \frac{\left(\frac{p_{d_i}}{p_{b_i}}\right)\left(\frac{T_{b_i}}{T_{d_i}}\right)}{\left[\frac{V^2}{6{,}088T_b} + 1\right]^{2.53}} \quad (21)$$

Now let C represent the parameter $[(V^2/6{,}088T_b) + 1]^{2.53}$. Then the supercharger-discharge density can be expressed in terms of the supercharger-entrance pressure, temperature and density by the equation

$$\delta_d = \left(\frac{p_b}{T_b}\right)\left(\frac{70.8}{R_i}\right)\theta C \quad (22)$$

or

$$\delta_d = \delta_b \theta C \quad (23)$$

For air, the pressure and temperature coefficients and density parameter are known to vary with the impeller load coefficient and may also be found to vary with initial temperature, especially at high impeller tip-speed values. However, for relatively small atmospheric pressure and temperature variations the supercharger pressure and temperature coefficients and density parameter can normally be assumed to remain constant. The ratio of standard to observed supercharger-discharge or blower-rim pressures, temperatures and densities then may be written:

$$\frac{p_{d_s}}{p_{d_i}} = \frac{p_{b_s}}{p_{d_i}}\left\{1 + \left[\left(\frac{p_{d_i}}{p_{b_i}}\right)^{0.283} - 1\right]\left(\frac{V_s}{V_i}\right)^2\left(\frac{T_{b_i}}{T_{b_s}}\right)\right\}^{3.54} \quad (24)$$

$$\frac{T_{d_i}}{T_{d_s}} = \frac{T_{d_i}}{(T_{d_i} - T_{b_i})(V_s/V_i)^2 + T_{b_s}} \quad (25)$$

$$\delta_{d_s}/\delta_{d_i} = (\delta_{b_s}/\delta_{b_i})(C_s/C_i) \quad (26)$$

By substitutions and combinations of Eqs. (14), (24), (25) and (26), the net theoretic effect of small changes in atmospheric conditions on the main-stage supercharger-discharge density, pressure and temperature, may now be evaluated for the full-throttle conditions of the single-stage engine.

For the test-stand corrections:

$$\frac{\delta_{d_s}}{\delta_{d_i}} = \left(\frac{p_{c_s}}{p_{c_i}}\right)\left(\frac{T_{c_i}}{T_{c_s}}\right)^{1/2}\left(\frac{C_s}{C_i}\right)\left[\frac{1 - (K_c V_{c_s}^2/T_{c_s})}{1 - (K_c V_{c_i}^2/T_{c_i})}\right] \quad (27)$$

$$\frac{p_{d_s}}{p_{d_i}} = \frac{p_{c_s}}{p_{d_i}}\left[1 - \left(\frac{T_{c_i}}{T_{c_s}}\right)\left(\frac{V_{c_s}}{V_{c_i}}\right)^2\left(1 - \frac{p_{b_i}}{p_{c_i}}\right)\right] \times \left[1 + (Y_i)\left(\frac{V_s}{V_i}\right)^2\left(\frac{T_{c_s}}{T_{c_i}}\right)^{1/2}\right]^{3.53} \quad (28)$$

$$\frac{T_{d_i}}{T_{d_s}} = \frac{T_{d_i}}{(T_{d_i} - 21.4T_{c_i}^{1/2})\left(\frac{V_s}{V_i}\right)^2 + 21.4T_{c_s}^{1/2}} \quad (29)$$

The pressure and temperature at the forward-facing intake air-scoop exit are evaluated in separate equations so that Eqs. (27) to (29) inclusive, as well as the air-scoop relations, may be used for other more complicated conditions. For the airplane installation, the ratios of observed and standard values of the carburetor entrance pressures and temperatures required by Eqs. (27) to (29) are given by Eqs. (11) and (12).

Intake Manifold Effect on the State of the Inducted Air

In the intake manifold, the inducted charge may be subjected to still further changes in pressure and temperature. A well-designed manifold will be the cause of only minor pressure losses which, ordinarily, can be assumed to be negligible. However, because of adverse heat transfer losses, fluid friction losses, and residual-gas blow back, an appreciable temperature rise may be found at the intake port. Fortunately, this temperature rise is generally found to be reproducible under any one set of operating conditions, although the magnitude of the temperature increase may vary considerably with engine speed and, to some degree, with cylinder cooling-air flow and cooling-air temperature changes.

Port-temperature variations with cooling conditions are almost impossible to predict with any accuracy.

Experience has shown, however, that this temperature function can be avoided by basing the cylinder pumping efficiency upon charge conditions at the main-stage supercharger outlet and by assuming that the same relative increase of charge temperature in the manifold will occur under both observed and standard operating conditions. This procedure is believed to be adequate if the engine is operated at about the desired normal cylinder temperatures during the test period. Failure to do this may result in port-temperature variations of as much as 3 per cent. The effect is sometimes shown up by differences in corrected output which occur when flying both on a single engine and on two engines of a bimotored airplane.

Volumetric Efficiency Variations with Atmospheric Changes

Zeyns' experiments[5] have shown the engine cylinder volumetric efficiency to be a function of the engine speed, the valve timing, the intake-charge temperature and the ratio of the exhaust pressure to intake-manifold pressure. Of these different factors, the intake-charge temperature effect is apparently of least importance and can generally be neglected. The relation of supercharger-discharge volumetric efficiency to the above factors can be determined only by experiment on the type of engine under consideration. A typical set of volumetric efficiency curves for a conventional aircraft engine with normal valve timing is shown by Fig. 3.

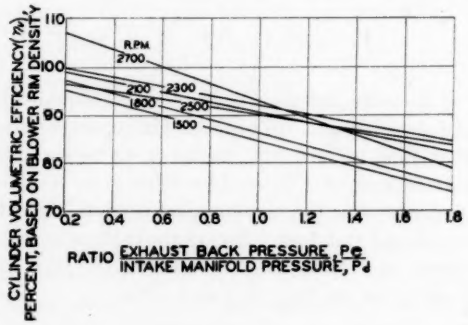

FIG. 3. Typical volumetric efficiency curves for a supercharged engine.

When operating under part-throttle conditions at constant pressure altitude, the ratio of exhaust back pressure can be expected to vary over a wide range of values, as the throttle opening and, hence, the manifold pressure is changed. This condition is typical of test-stand or sea-level dynamometer operation. Also, at constant manifold pressure and varying altitude conditions—i.e., varying exhaust back pressure—the manifold-to-back-pressure ratio is subject to rather wide variations. However, for a single-stage supercharged engine under full-throttle operation, the ratio of manifold pressure to exhaust back pressure is substantially equal to the overall compression ratio of the supercharging system. This is, in turn, a function of the impeller tip speed and the initial temperature at the supercharger entrance. As the ratio of exhaust pressure to supercharger-discharge pressure remains substantially constant for the full-throttle condition, the full-throttle volumetric efficiency of a single-stage engine, operating at fixed engine speed, can be assumed to remain substantially constant regardless of changes in atmospheric pressure or temperature.

If it is desired to take the volumetric efficiency factor into account and if it is assumed that the observed and standard values of both the main stage supercharger-discharge pressure and the exhaust back pressure have been either measured or calculated, the corresponding observed and standard values of the cylinder volumetric efficiency may be found by reference to a curve similar to that in Fig. 3. The curve must be supplied by the engine manufacturer for the engine under consideration. On this curve the observed and standard values of volumetric efficiency corresponding to the observed and standard values of the parameter (p_e/p_d) are spotted for the engine speed at which the power correction is being made.

Recent experiments have indicated that the volumetric efficiency may be varied as much as 2 to 4 per cent by wide changes in cylinder operating temperatures. Those changes are believed to be due largely to variations in tappet clearance as the cylinders expand or contract. The effects of tappet clearance changes on output are unpredictable; therefore it is again suggested that attempts be made to test at the expected cylinder-operating temperatures, if possible, to eliminate errors due to cylinder temperature effects.

Mixture Strength and Specific Air Consumption Variations with Atmospheric Changes

In an aircraft engine equipped with a fully automatic carburetor, the indicated specific air consumption and the mixture strength are normally independent of atmospheric conditions at the entrance of the induction system. The fuel-air-mixture ratio depends only upon the carburetor setting and the accuracy of the automatic altitude and economizer controls, and the specific air consumption is dependent primarily upon the mixture ratio.

Unless the engine under test has been operated at other than the desired mixture-strength setting during the test period, there should ordinarily be no correction for fuel-air ratio or specific air consumption. However, under certain conditions of operation with automatic carburetors, this may not be the case. Fig. 6 illustrates a typical carburetor setting curve for an aircraft engine equipped with an automatically compensated carburetor. Should the engine be operating in either the "idle-transfer" or "economizer" ranges under the conditions of test, then the correction to standard atmospheric conditions will involve not only a change in output, because of the change in inducted airflow, but also some change in output due to the change in mixture strength

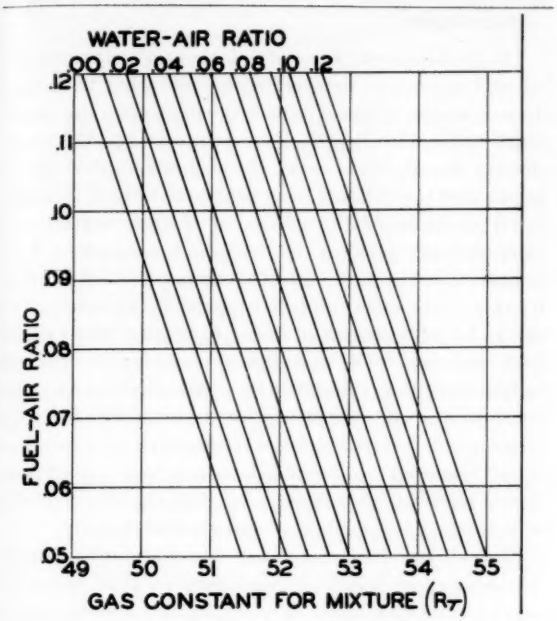

FIG. 4. Relation of intake charge gas constant (R_i) to fuel-air ratio and intake charge moisture content.

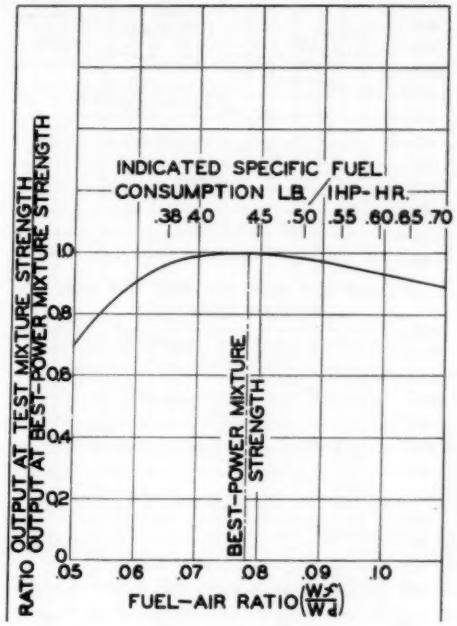

FIG. 5. Empirical curve for correcting indicated output for fuel-air ratio changes.

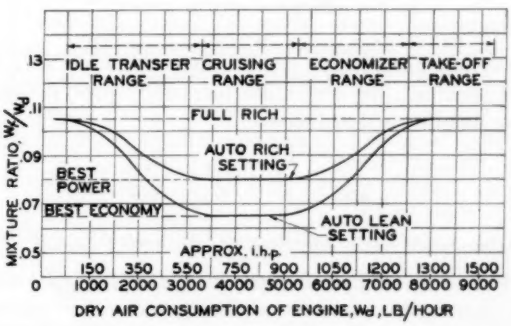

FIG. 6. Typical carburetor-setting curve for an aircraft engine.

which accompanies the change in airflow. It is apparent that not only the carburetor setting curve for the engine under consideration but also an estimate of the air consumption at test and standard conditions is required for correction of output to standard atmosphere under these conditions.

Inasmuch as specific air consumption and fuel-air ratio are closely interrelated, it is convenient to consider these two factors together rather than as separate entities.

If all other factors of Eq. (6) are considered to remain constant, the variation of indicated horsepower with both mixture strength and specific air consumption becomes

$$\frac{\text{i.hp.}_s}{\text{i.hp.}_i} = \frac{\text{i.s.a.c.}_i\,[1 + (W_f/W_d)]_i}{\text{i.s.a.c.}_s\,[1 + (W_f/W_d)]_s} \qquad (30)$$

Because the indicated specific air consumption must be determined experimentally anyway, it is convenient to determine by tests the empirical ratio of the i.hp. at any given mixture strength to the i.hp: at best-power mixture strength and to plot this ratio at the test mixture-strength value. This procedure implies that best-power mixture strength is the "standard" mixture. An experimentally determined curve of this sort is presented to permit corrections to best-power mixture strength (see Fig. 5).

Atmospheric Moisture-Content Effects

Within the induction system the moisture content of the inducted air, in terms of the mass weight of water relative to the mass weight of air, can be expected to remain constant, unless, of course, induction-system icing occurs. However, the density of the inducted charge may be appreciably affected by water-vapor content as well as by the supercharger, carburetor, etc.

Under standard atmospheric conditions, based on N.A.C.A. standard air, the water-vapor content is assumed to be zero and the term $[1 + (W_w/W_d)]_s$ is equal to unity. The gas constant, which relates the inducted charge density to the pressure, temperature, water-vapor content and the fuel content of the charge may be determined by use of Fig. 4. The standard gas-content value always lies on the extreme left line of this figure.

The observed water-vapor content may be measured by means of such instrumentation as a hair hygrometer, wet-and-dry-bulb thermometer readings or a dew-point indicator. The ratio $(W_w/W_d)_i$ may then be found from any convenient psychometric chart with proper

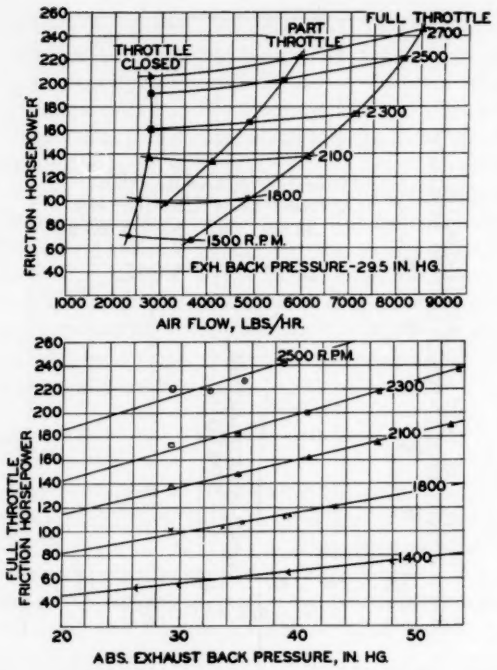

FIG. 7. Variation of friction horsepower with engine speed, throttle setting and exhaust pressure.

corrections for altitude effect. Assuming all other factors constant, the correction for water vapor content may be expressed as follows:

$$\frac{\text{i.hp.}_s}{\text{i.hp.}_i} = \left(1 + \frac{W_w}{W_d}\right)_i \left(\frac{R_{ti}}{R_{ts}}\right) \tag{31}$$

Engine-Speed Variations with Atmospheric Changes

Practically all modern aircraft that are equipped with supercharged engines are also equipped with constant-speed propellers. The constant-speed propeller regulates the engine crank speed to the desired value regardless of changes in atmospheric pressure temperature or density; therefore the ratio of standard to observed engine speed (N_s/N_i) can ordinarily be assumed to be equal to unity. In some cases, however, it may be found that, because of oversight or a faulty tachometer, the engine was not operated at the desired crank speed and the effect of an engine-speed correction is desired. For this case the indicated engine-speed value is known and the standard engine-speed value is assumed. In making an engine-speed correction, it must be remembered that corresponding changes in supercharger tip speed must be included in the correction formulas. For gear-driven single-stage superchargers

$$V_s = V_i(N_s/N_i) \tag{32}$$

and for the gear-driven auxiliary-stage supercharger, to be discussed later,

$$V_{1s} = V_{1i}(N_s/N_i) \tag{33}$$

Atmospheric Effects on Friction Horsepower of a Single-Stage Engine

The friction horsepower of a single-stage supercharged aircraft engine, as determined by motoring tests on a dynamometer, is found to be dependent upon the engine crank speed, the oil and engine temperatures, the supercharger impeller-gear ratio, the airflow inducted by the engine and the exhaust back pressure. Fig. 7 is a typical illustration of the effects of throttle setting and exhaust back pressure on friction horsepower. It is notable that the major effect of atmospheric changes on friction horsepower, all other factors being constant, is shown by the variation of motoring friction with exhaust back pressure. The variation of motoring friction with inducted airflow is found to be small with respect to the total friction and can be neglected for the small changes in inducted airflow which are represented by corrections from observed to standard atmospheric conditions. Minor oil or engine temperature changes are of negligible effect unless scavenging is also affected thereby.

For all practical purposes, the relation of friction horsepower at standard conditions to that under observed conditions may be assumed to be a function of the exhaust back pressure only. The friction horsepower variation must be determined experimentally on a motoring dynamometer until more is known concerning the laws governing the effect of back pressure upon motoring friction.

Single-Stage Engine Full-Throttle Power Correction Formulas

By taking into account the effects of atmospheric changes on engine speed, friction horsepower, and the performance of various induction-system units, the theoretic full-throttle power-correction formula for a single-stage supercharged engine with constant-speed propeller may now be written as follows:

$$\text{b.hp.}_s = [\text{b.hp.}_i + \text{f.hp.}_i]\left[\frac{N_s}{N_i}\right]\left[\frac{\eta_{vs}}{\eta_{vi}}\right]\left[\frac{p_{cs}}{p_{ci}}\right]\left[\frac{T_{ci}}{T_{cs}}\right]^{1/2} \times$$

$$\left[\frac{C_s}{C_i}\right]\left[\frac{1-(K_c V_{cs}^2/T_{cs})}{1-(K_c V_{ci}^2/T_{ci})}\right]\left[\frac{\text{i.s.a.c.}_i}{\text{i.s.a.c.}_s}\right]\left[\frac{\left(1+\frac{W_f}{W_d}\right)_i}{\left(1+\frac{W_f}{W_d}\right)_s}\right] \times$$

$$\left[\left(1+\frac{W_w}{W_d}\right)_i\right]\left[\frac{R_{ti}}{R_{ts}}\right] - \text{f.hp.}_s \tag{34}$$

This relation may be simplified considerably by assuming: (1) that the engine was tested at the desired engine speed—N_s/N_i = unity and V_s/V_i = unity; (2) that the exhaust-manifold back-pressure change is of small magnitude—η_{vs}/η_{vi} = unity and $\text{f.hp.}_s = \text{f.hp.}_i$; (3) that the full-throttle loss through the carburetor is so small as to be of negligible effect, $[1-(K_c V_{cs}^2/T_{cs})]/[1-(K_c V_{ci}^2/T_{ci})]$ = unity; (4) that the mixture ratio is of the desired value and will not change appreciably because of economizer or idle-transfer action.

The above assumptions result in a simplified single-stage full-throttle formula, as follows:

$$\text{b.hp.}_s = [\text{b.hp.}_t + \text{f.hp.}_t] \times \left[\frac{p_{cs}}{p_{ci}}\left(\frac{T_{ci}}{T_{cs}}\right)^{1/2}\frac{C_s}{C_i}\left(1+\frac{W_w}{W_d}\right)_t\frac{R_{ti}}{R_{ts}}\right] - \text{f.hp.}_t \quad (35)$$

For altitudes above 5,000 ft. the moisture content of the air is generally low, so the terms $1 + (W_w/W_d)$ and R_{ti}/R_{ts} may also be omitted. These terms are generally much more important for dynamometer corrections than for flight-test corrections.

When the engine is installed in an airplane, the values of p_{cs}/p_{ci} and T_{ci}/T_{cs} are determined by Eqs. (11) and (12). For convenience, the chart of Fig. 8 is presented for the determination of the parameter C.

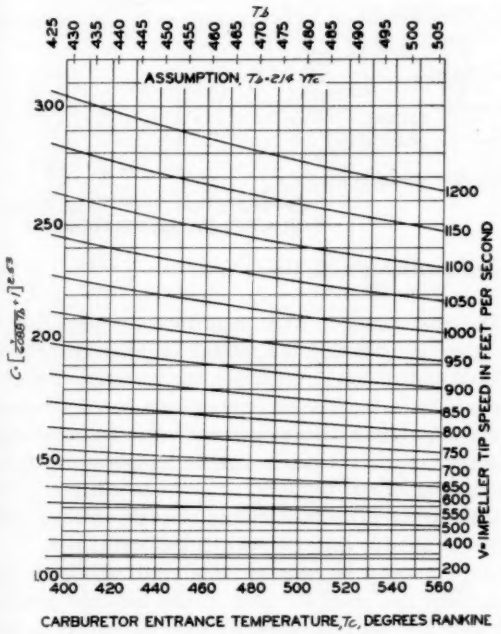

FIG. 8. Chart for rapid determination of the parameter "C."

Part-Throttle Single-Stage Correction Formulas

At part throttle, for which condition the intake-manifold pressure is assumed to remain constant, a theoretic power-correction formula can be written as follows:

$$\text{b.hp.}_s = [\text{b.hp.}_t + \text{f.hp.}_t]\left[\frac{N_s}{N_i}\right]\left[\frac{\eta_{vs}}{\eta_{vi}}\right]\left[\frac{T_{di}}{T_{ds}}\right]\left[\frac{\text{i.s.a.c.}_i}{\text{i.s.a.c.}_s}\right] \times \left[\frac{\left(1+\frac{W_f}{W_d}\right)_t}{\left(1+\frac{W_f}{W_d}\right)_s}\right]\left[\left(1+\frac{W_w}{W_d}\right)_t\right]\left[\frac{R_{ti}}{R_{ts}}\right] - \text{f.hp.}_s \quad (36)$$

For substitution in this formula, the ratio T_{di}/T_{ds} has been evaluated in terms of T_{ci} and T_{cs} by Eq. (29).

If the same simplifying assumptions are made for the part-throttle condition that were made for the full-throttle condition, the theoretic part-throttle correction formula may be reduced to the simplified form:

$$\text{b.hp.}_s = [\text{b.hp.}_t + \text{f.hp.}_t]\left[\frac{T_{di}}{T_{di} - 21.4(T_{ci}^{1/2} - T_{cs}^{1/2})}\right] \times \left[\left(1+\frac{W_w}{W_d}\right)_t\right]\left[\frac{R_{ti}}{R_{ts}}\right] - \text{f.hp.}_t \quad (37)$$

It will be shown later that part-throttle Eq. (37) is correct in form but that the temperature term is incorrect because of other factors not taken into account in the derivation of the equation.

Experimental Checks of the Single-Stage Power Correction Formulas

In order to check the rationally developed single-stage power correction formulas, two special test setups were made. An engine was first thoroughly calibrated on an electric cradle dynamometer stand after which it was installed in a Vultee AB-2 airplane. The power plant used for the investigation was a Pratt & Whitney R-1830 engine equipped with a single-stage two-speed supercharger.

Besides the usual calibrated engine instruments, several items of special equipment were installed to permit the measurement and control of the following:

Item	Instrumentation	Control
Engine speed	Sensitive tachometer	(d) Electric dynamometer (a) Constant speed propeller
Engine output	(d) Cradle dynamometer (a) Torquemeter and gauge	Throttle, etc.
Induction system pressure	(d) Mercury manometers (a) Sensitive manifold pressure gauge	(d) Air chute throttle (a) Altitude change
Induction system temperatures	(a) Thermocouples & and (d) Potentiometer	(a) Carburetor preheat system
Exhaust system pressure	(d) Mercury manometer (a) Sensitive manifold pressure gauge	(a) Throttle in exhaust manifold & (d) tail pipe
Induction system airflow	(a) Calibrated orifice & and (d) pressure gauge	(a) Throttle and density change (altitude and preheat) & (d)
Cylinder temperatures	(a) Thermocouples & and (d) Potentiometer	(d) Cooling blower throttle (a) Cowl flaps

NOTE: (a) represents airplane installation and (d) represents dynamometer installation.

The airplane test setup is illustrated by Fig. 9.

On the dynamometer, numerous so-called "altitude" calibrations were made for varying conditions of exhaust back pressure, mixture ratio, cylinder cooling, carbu-

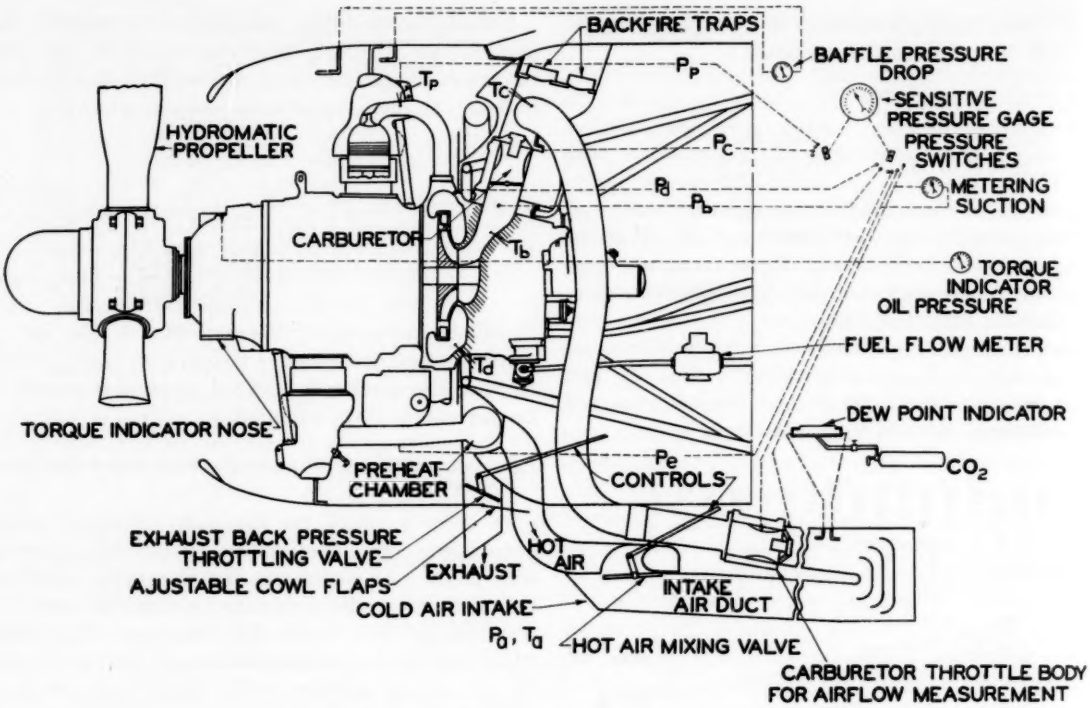

FIG. 9. Flight test setup for power correction-factor investigations.

retor-entrance pressure, impeller-gear ratio and engine speed. Because of unsatisfactory carburetor-air temperature control, the dynamometer tests were all made at a constant carburetor-air temperature of 90°F.

The flight tests consisted of full-throttle runs at 1,800 and 2,300 engine r.p.m. at altitudes of 5,000, 10,000, 14,000 and 18,000 ft. At each altitude the supercharger was operated in both low and high impeller-gear ratios. At 5,000 and 10,000-ft. altitudes, the variation of engine output with carburetor-air temperature was determined by varying the carburetor preheat valve from full-cold to full-hot positions, the range of temperatures being of the order of 60° to 80°F. at any one altitude. For these runs, the exhaust-manifold throttle valve, as well as the carburetor throttle, was locked wide open.

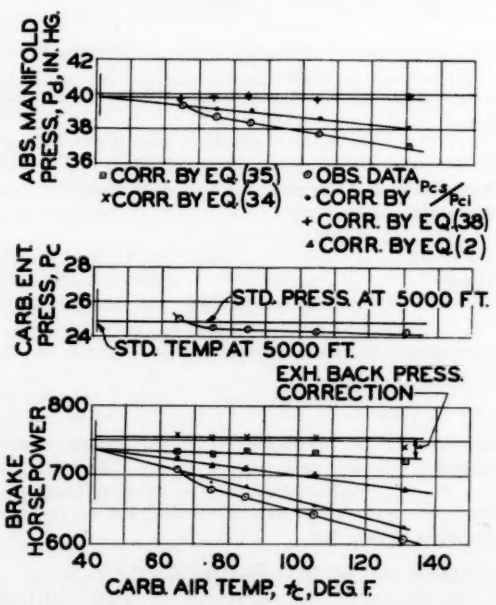

FIG. 10. Typical performance and output-correction curves obtained during temperature-test investigations.

Another series of runs at 5,000 and 10,000 ft. was made with the preheat valve in the full-cold position and with the exhaust-manifold throttle varied to produce back-pressure changes of as much as 15 in. Hg.

For all tests, the engine cylinder temperatures were kept at about the normal value for continuous operation (450°F.) by control of cowl flaps. The carburetor mixture was controlled manually to obtain "best power" setting at each operating point.

At each different test condition, the induction system pressures, and temperatures, the cylinder temperatures and baffle-pressure head, the engine speed and output, the exhaust-system pressure, the inducted airflow, fuel flow and water-vapor content were measured and recorded.

The test data taken for varying carburetor-air temperatures were plotted as shown by the typical curves of Fig. 10. Corrections to standard pressure and temperature at the carburetor entrance were made to the observed engine output values, using the precise Eq. (34), the simplified Eq. (35) and the generally-used Eq.

(2). The manifold pressure was also corrected to standard conditions by use of a simplified form of Eq. (28)—namely,

$$p_{d_2} = p_{c_2} \left\{1 + \left[Y_f \left(T_{c_1}/T_{c_2}\right)^{1/4}\right]\right\}^{3.53} \qquad (38)$$

The results of these corrections are also shown on Fig. 10. The superiority of the proposed full-throttle Eqs. (34) and (35) to the generally used Eq. (2) is to be noted.

Typical results of the back-pressure runs are shown by Fig. 11. Each point on this curve was corrected to standard atmospheric back-pressure conditions by correcting, first, for volumetric efficiency variations with p_e/p_d and, second, for friction horsepower variations with p_e. The experimental volumetric efficiency and friction-horsepower data used for these corrections were determined from the extensive test-stand runs on the engine (Figs. 3 and 7). The excellence of the back-pressure correction method is also to be noted.

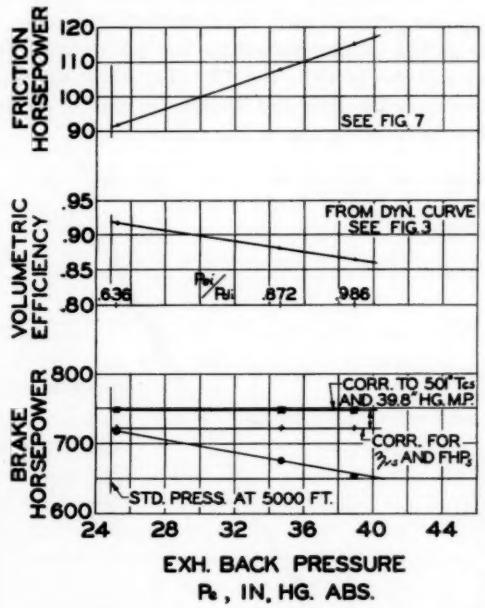

FIG. 11. Typical performance and output-correction curves obtained during back-pressure test investigations.

In order to check the assumptions that the supercharger pressure and temperature coefficients and the density parameter remain sufficiently constant during power correction periods to justify the correction formulas, the experimentally determined values were plotted against the carburetor-entrance temperature, as shown by Fig. 12. It is notable that for any fixed engine speed the pressure coefficient and density parameter remained substantially constant regardless of carburetor air temperature. However, the temperature coefficient was found to vary over a wide range of values, some of which were unbelievable.

To determine the cause of this extreme variation of temperature coefficient with carburetor-entrance temperature, all induction-system temperatures were plotted against carburetor-entrance temperature as shown by Fig. 13. Inspection of these plots led to the conclusion that for low carburetor-entrance temperature values the fuel continues to vaporize as it passes through the impeller and diffuser. This gives an effective temperature drop, below the carburetor air temperature, very much as indicated by the lower dashed line in Fig. 13.

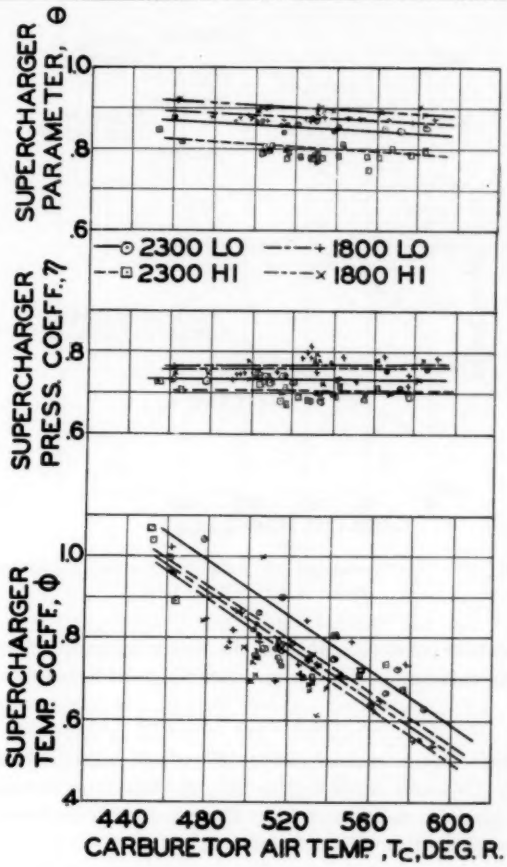

FIG. 12. Test variations of supercharger coefficients as obtained during flight tests.

For best-power mixture, this effective drop amounts to about 70°F. at an initial carburetor air temperature of 130°F., and 45°F. at a carburetor air temperature value of 0°F. For the engine model tested, a formula of the form

$$T_b = 0.812(T_c + 50) \qquad (39)$$

expresses the relation of the effective supercharger-entrance temperature with respect to the carburetor-entrance temperature.

The relation of observed to standard effective impeller-entrance temperature for the above relation becomes:

$$T_{b_1}/T_{b_2} = (T_{c_1} + 50)/(T_{c_2} + 50) \qquad (40)$$

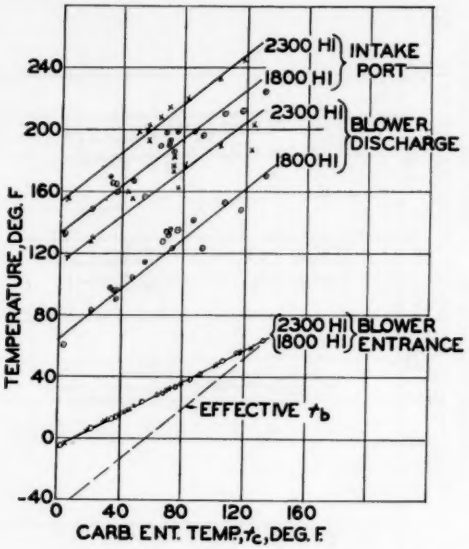

FIG. 13. Test variations of induction-system temperatures obtained during flight tests.

and a revised formula for the supercharger-discharge temperature at constant impeller tip speed is as follows:

$$T_{di}/T_{ds} = T_{di}/[T_{di} + 0.812(T_{cs} - T_{ci})] \qquad (41)$$

This relation, instead of Eq. (29), when combined with Eq. (36) and simplified as before, should be expected to give a more accurate part-throttle correction formula to replace Eq. (37) as follows:

$$\text{b.hp.}_s = [\text{b.hp.}_i + \text{f.hp.}_i] \times \left[\frac{T_{di}}{T_{di} + 0.812(T_{cs} - T_{ci})}\right]\left[1 + \frac{W_w}{W_d}\right]_i \left[\frac{R_{ti}}{R_{ts}}\right] - \text{f.hp.}_i \qquad (42)$$

PART-THROTTLE CORRECTION FORMULA CHECKS

In order to check the part-throttle, constant manifold pressure, formulas by use of the full-throttle test data of Fig. 10, the engine output at the different carburetor air temperatures of this figure were first corrected to constant manifold pressure by the relation:

$$\text{b.hp.}_{(corr.)} = (\text{b.hp.}_i + \text{f.hp.}_i)(p_{ds}/p_{di}) - \text{f.hp.}_i \qquad (43)$$

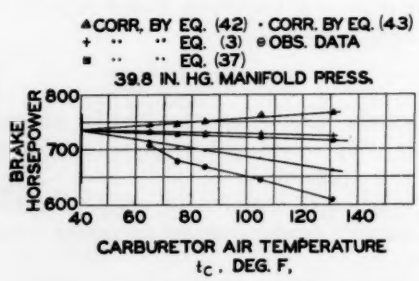

FIG. 14. Checks of part-throttle, correction-factor formulas.

For this relation the value of p_{ds} was assumed to be 39.8 in. Hg. A plot of these pressure-corrected output values is shown on Fig. 14. The part-throttle correction formulas were next applied to the above-plotted output values. These results are also shown on Fig. 14 and the relative accuracy of the various formulas is demonstrated.

It is apparent that neither of the rational part-throttle formulas gave as good accuracy as the empirical Eq. (3). The three part-throttle formulas were also applied to test data taken on other engine models. In practically all cases, empirical Eq. (3) was as good as or better than either Eq. (37) or Eq. (42).

Check of Assumptions in Derivation of Formulas

Several other plots of the test data were made to check some of the basic assumptions made in the derivation of the correction formulas. In order to check Eq. (4), all the indicated horsepower values obtained at best-power mixture ratio were plotted against the dry mass airflow as determined by the calibrated orifices. The results are given in Fig. 15. The direct linear relation between the indicated horsepower and the dry mass airflow justifies the use of Eq. (4).

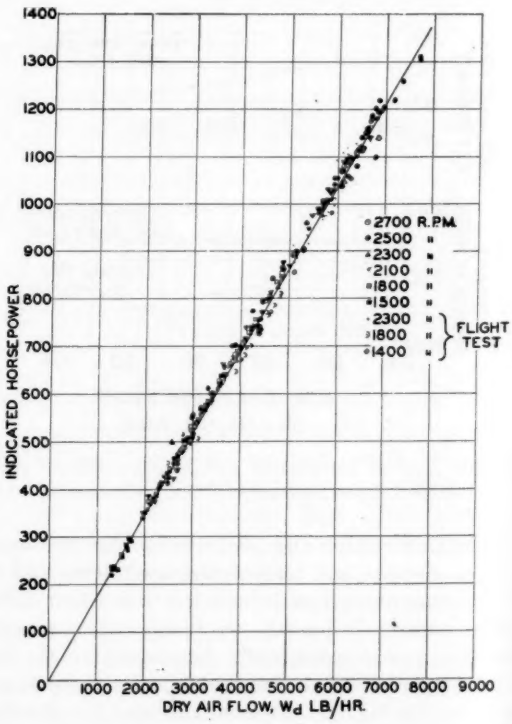

FIG. 15. Linear variation of indicated horsepower with dry mass airflow.

The relation of indicated specific air consumption to fuel-air ratio, engine speed, output, etc., was found by plotting several test i.s.a.c. values against mixture ratio for the various engine-speed and engine-output values

tested. This plot, Fig. 16, indicates that the mixture ratio is the major variable affecting the indicated specific air consumption. Variations of i.s.a.c. due to engine speed and engine output were practically within the experimental error of testing.

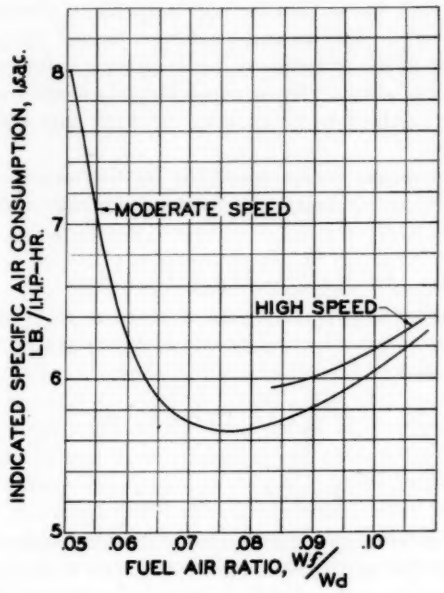

FIG. 16. Variation of indicated specific air consumption with fuel-air mixture ratio.

The curves of Figs. 2, 3, 5 and 7 were also the results of plotting the test data obtained during the dynamometer and flight tests.

Because of the generally satisfactory correlation between the theoretic formulas and the experimental results obtained on the single-stage engine, theoretic studies of correction formulas for two-stage engines with gear-driven and turbo-driven auxiliary stages were continued. Unfortunately, no carefully controlled flight-test checks of these formulas were possible.

CORRECTION FORMULAS FOR THE TWO-STAGE SUPERCHARGED ENGINE

The induction system of a typical airplane installation of an engine, equipped with a two-stage gear-driven supercharger, is illustrated in Fig. 17. Between the carburetor and the intake air scoop of the single-stage engine another supercharger and an intake-charge intercooler have been added. At full-throttle conditions, the ram-scoop-exit pressure and temperature are substantially equal to the pressure and temperature at the entrance of the auxiliary-stage impeller. That is, $p_{b_1} = p_r$ and $T_{b_1} = T_r$. Eqs. (9) and (10) again may be used to calculate the values of T_r and p_r.

The pressure and temperature at the auxiliary-stage outlet can be determined by relations similar to those of Eqs. (18) and (19):

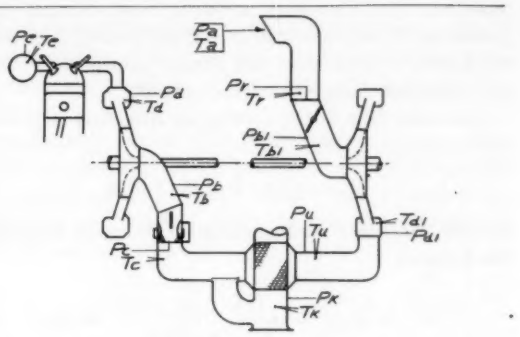

FIG. 17. Typical induction system of a two-stage engine with direct gear-driven auxiliary stage.

$$\frac{p_{d_1}}{p_{b_1}} = \frac{p_{d_1}}{p_r} = \left(\frac{\eta_1 V_1^2}{6{,}088 T_r} + 1\right)^{3.53} \tag{44}$$

and

$$\frac{T_{d_1}}{T_{b_1}} = \frac{T_{d_1}}{T_r} = \left(\frac{\eta_1 V_1^2}{\phi_1\, 6{,}088 T_r} + 1\right) \tag{45}$$

For the auxiliary-stage supercharger the use of a density parameter θ is unwarranted, since the pressures and temperatures must be considered as separate entities in correcting to standard conditions.

On passing through the intercooler, the air discharged from the auxiliary-stage supercharger undergoes both a pressure and temperature change. The pressure change is largely dependent upon the air density and the mean velocity at the induction-air face of the intercooler, whereas the temperature drop is dependent upon the temperature and mass flow of cooling air passing through the intercooler in the cross-flow direction.

The pressure drop of the inducted air passing through the intercooler may be determined by a relation similar to that of Eq. (13)

$$p_{d_1} - p_c = K_u p_{d_1} V_u^2 / T_{d_1} \tag{46}$$

In estimating the variation of the engine air temperature drop through the intercooler due to atmospheric changes, it is necessary to make some assumptions concerning the change in cooling air conditions in the intercooler as well as the change in engine air conditions.

At a fixed ratio of mass cooling airflow to mass engine airflow, the intercooler effectiveness, e, is given by the relation:

$$e = (T_{d_1} - T_c)/(T_{d_1} - T_k) \tag{47}$$

This intercooler effectiveness can be expected to remain substantially constant over a reasonably wide range of pressure and temperature conditions if the ratio of inducted engine airflow to cooling airflow does not change appreciably.

For relatively small changes of atmospheric pressure and temperature, this latter condition will be found to be approximately true *if the overall conductivity of the*

intercooler and its cooling air duct is not changed by the movement of the cooling-duct exit-gill-control flap and if the airplane speed does not change appreciably due to the expected change in engine output.

The mass flow in the cooling air direction is given by the formula:

$$W_k = Q_k\delta_k = C_kK_kS_kV_a\delta_k \tag{48}$$

and the mass flow in the engine air direction is given by the formula:

$$W_u = Q_u\delta_u = \sqrt{\frac{141.6(p_{d_1} - p_c)}{\delta_u/32.17}}\,K_uS_u\delta_u \tag{49}$$

From Eq. (46)

$$p_{d_1} - p_c = 0.754\delta_uK_uV_u^2 \tag{50}$$

Therefore,

$$W_u = 58.5K_u^{2/3}S_uV_u\delta_u \tag{51}$$

and

$$\frac{W_k}{W_u} = \frac{C_kK_kS_kV_a\delta_k}{58.5K_u^{2/3}S_uV_u\delta_u} = \text{Const.} \times \frac{V_a\delta_k}{V_u\delta_u} \tag{52}$$

At constant engine speed and full-throttle setting, the mean velocity of the air at the intercooler engine air face (V_u) will be found to be relatively independent of atmospheric density changes in the induction system, and both δ_u and δ_k will vary approximately in proportion to the atmospheric air density δ_a. If the airplane velocity change is also assumed to be negligible, it is apparent that the ratio of cooling airflow to inducted engine airflow is approximately constant and the function e may also be assumed to be constant for correction formula derivations.

If Eq. (47) is now solved for T_c the result is:

$$T_c = T_{d_1}(1 - e) + eT_k \tag{53}$$

Inspection of Eqs. (12) and (44) will show that for constant auxiliary-stage impeller tip speed and for the small changes in airplane speed and scoop-exit velocity ordinarily involved in correcting engine output to standard conditions the temperature rise in the ram scoop and in the auxiliary-stage supercharger remains constant regardless of initial temperature or pressure. Similar reasoning will show that the temperature rise of the intercooler cooling air, as it enters the cooling air-entrance duct, also remains substantially constant regardless of initial air temperature or pressure.

These statements may be expressed algebraically as follows:

$$T_{d_1} = \text{Const.}_1 + \text{Const.}_2 + T_u \tag{54}$$

and

$$T_k = \text{Const.}_3 + T_a \tag{55}$$

The substitution of these values in Eq. (53) gives the following equation:

$$T_c = (\text{Const.}_1 + \text{Const.}_2)(1 - e) + (1 - e)T_a + e\,\text{Const.}_3 + eT_a \tag{56}$$

or

$$T_c = T_a + \text{Const.}_4 \tag{57}$$

Eq. (57) shows that for the purposes of correcting engine output to standard conditions the net temperature rise of the atmospheric air in passing through the ram scoop, auxiliary-stage supercharger and intercooler can be assumed to be constant at fixed engine-speed condition.

For constant engine speed the relation of observed to standard carburetor air temperature may now be written:

$$T_{ci}/T_{cs} = T_{ci}/(T_{ci} - T_{ai} + T_{as}) \tag{58}$$

Also, the standard temperatures in other parts of the auxiliary-stage induction system may be calculated by the relations

$$T_{d_{1s}} = T_{d_{1i}} - T_{ai} + T_{as} \tag{59}$$

and

$$T_{rs} = T_{ri} - T_{ai} + T_{as} \tag{60}$$

These latter temperatures must be used in determining the standard pressures at various locations in the induction system. The standard pressure at the auxiliary-stage discharge is given in terms of the ram-scoop pressure and temperature by a relation similar to Eq. (24):

$$p_{d_{1s}} = p_{rs}[1 + (Y_{1i})(V_{1s}/V_{1i})^2(T_{ri}/T_{rs})]^{3.53} \tag{61}$$

The standard pressure at the carburetor entrance may also be given in terms of the auxiliary-stage discharge pressure and temperature by the relation:

$$p_{cs} = p_{d_{1s}}\left[1 - \left(\frac{p_{d_{1i}} - p_{ci}}{p_{d_{1i}}}\right)\left(\frac{T_{d_{1i}}}{T_{d_{1s}}}\right)\left(\frac{V_{us}}{V_{ui}}\right)^2\right] \tag{62}$$

The simplifying assumptions that changes in airplane speed, scoop-exit velocity and induction-air velocity at the intercooler engine air face are negligible may now be made, and Eqs. (11), (12), (58), (59), (60), (61) and (62) may be combined to give the relation

$$\frac{p_{cs}}{p_{ci}} = \frac{p_{as}}{p_{ci}}\left[1 + Y_{ri}\left(\frac{T_{ai}}{T_{as}}\right)\right]^{3.53} \times \left[1 + Y_{1i}\left(\frac{T_{ri}}{T_{ri} - T_{ai} + T_{as}}\right)\right]^{3.53} \times \left[1 - \left(\frac{p_{d_{1i}} - p_{ci}}{p_{d_{1i}}}\right)\left(\frac{T_{d_{1i}}}{T_{d_{1i}} - T_{ai} + T_{as}}\right)\right] \tag{63}$$

This equation may be combined with Eqs. (58) and (35) to obtain a somewhat complicated full-throttle correction formula for airplane-installed engines equipped with gear-driven two-stage superchargers:

$$\text{b.hp.}_s = \{\text{b.hp.}_i + \text{f.hp.}_i\}\left\{\frac{p_{as}}{p_{ci}}\left[1 + Y_{ri}\left(\frac{T_{ai}}{T_{as}}\right)\right]^{3.53} \times \left[1 + Y_{1i}\left(\frac{T_{ri}}{T_{ri} - T_{ai} + T_{as}}\right)\right]^{3.53} \times \left[1 - \left(\frac{p_{d1i} - p_{ci}}{p_{d1i}}\right)\left(\frac{T_{d1i}}{T_{d1i} - T_{ai} + T_{as}}\right)\right] \times \left[\frac{T_{ci}}{T_{ci} - T_{ai} + T_{as}}\right]^{1/2}\left[\frac{C_s}{C_i}\right]\left[1 + \frac{W_w}{W_d}\right]_i\left[\frac{R_{ti}}{R_{ts}}\right]\right\} - \text{f.hp.}_s \quad (64)$$

It is notable that it is necessary to know the test values of practically all the induction-system pressures and temperatures in order to correct the two-stage engine output to standard conditions.

Eq. (64) covers the case in which the cooling air passing through the two-stage engine intercooler is unregulated by intercooler cooling air control flaps. If either automatic or manual control of the cooling air to the intercooler is assumed, it is reasonable to suppose that such control will be for the purpose of obtaining constant carburetor air temperature. When carburetor air temperature control is assumed, atmospheric pressure and temperature changes will affect only the carburetor-entrance pressure. In order to correct the two-stage full-throttle engine output to standard conditions under this type of operation, the terms $[T_{ci}/(T_{ci} - T_{ai} + T_{as})]^{1/2}$ and C_s/C_i of Eq. (64) should be dropped.

A full-throttle correction formula for a dynamometer installation of a two-stage engine has not been derived, since the two-stage engine is ordinarily supercharged so highly that full-throttle operation at or near sea level is impossible because of engine strength and detonation limitations.

When a two-stage engine is tested on a dynamometer with the auxiliary stage in operation, the air-throttle and carburetor-entrance temperatures are either regulated to standard atmospheric pressure and temperature conditions or the carburetor-entrance pressure is regulated to the desired value and corrections are made only for carburetor air temperature and back-pressure variations from standard. These corrections simulate the so-called part-throttle corrections for the flight installation.

Part-Throttle Correction Factors for Gear-Driven Two-Stage Engines in Flight

The two-stage engine, when operating below its maximum critical altitude, may be in "neutral," "low auxiliary" or "high auxiliary" condition.

When the engine is operating in the neutral condition, it is essentially comparable to a single-stage engine, with the exception that for the neutral condition scoop losses, from atmospheric air pressure to carburetor air pressure, are likely to be relatively large. For flights up to the main-stage critical altitude, with the auxiliary stage in neutral, the correction Eq. (42) applies. Above the main-stage critical altitude Eq. (35) applies until the auxiliary stage is shifted into the low-auxiliary condition.

Immediately after this shift is made, an automatic carburetor-entrance pressure control is brought into operation, so that below the low-auxiliary critical altitude $p_{cs} = p_{ci}$ and the part-throttle correction formula becomes:

$$\text{b.hp.}_s = [\text{b.hp.}_i + \text{f.hp.}_i]\left[\left(\frac{T_{ci}}{T_{ci} - T_{ai} + T_{as}}\right)^{1/2} \times \left(\frac{C_s}{C_i}\right)\left(1 + \frac{W_w}{W_d}\right)_i\left(\frac{R_{ti}}{R_{ts}}\right)\right] - \text{f.hp.}_i \quad (65)$$

For this case the assumption that the temperature rise from the outside air to the carburetor entrance is constant is probably not quite so justified as it is for the full-throttle condition. For the part-throttle condition the ratio of mass airflows through the two respective entrance faces of the intercooler probably does not remain so constant as it does for the full (air) throttle condition.

On reaching the full-throttle condition in low-auxiliary stage the automatic carburetor-entrance pressure control becomes inoperative and Eq. (64) applies.

When the auxiliary-stage impeller is next shifted into high-auxiliary position, the automatic carburetor-entrance pressure control again becomes operative and Eq. (65) applies up to the full air-throttle opening position, when Eq. (64) again applies.

In using the above-mentioned correction formulas, it must be remembered that the observed friction horsepower, f.hp.$_i$, and the auxiliary-stage impeller tip-speed change to a different value at each different auxiliary-supercharger operating condition.

Correction Formulas for Turbosupercharged Engines

Fig. 18 illustrates a typical induction-system diagram for a two-stage engine with a turbo-driven auxili-

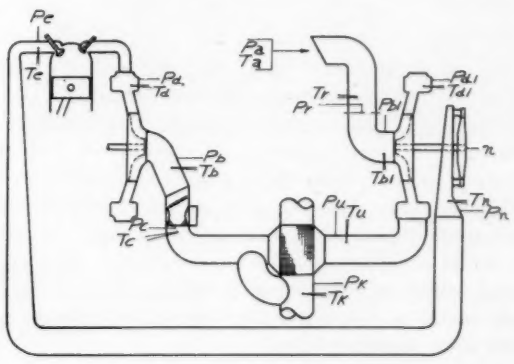

FIG. 18. Typical induction system of a two-stage engine with turbo-driven auxiliary stage.

ary-stage supercharger. As far as correction formulas are concerned the basic difference between the turbo-driven and the gear-driven superchargers lies in the fact that the tip speed of the turbosupercharger impeller does not necessarily remain constant, even though the engine speed may be held constant. When the turbo is in operation below critical altitude, the automatic turbo-control is ordinarily adjusted to maintain a constant manifold pressure by varying the turbo-exhaust gas waste gate position. Critical altitude for the turboengine generally occurs when maximum allowable turbowheel tip speed is reached. It may be assumed that above critical altitude the turbowheel and turbosupercharger impeller tip speed is regulated to a substantially constant limiting value and that Eq. (64) applies in output corrections.

In this case constant engine-speed operation is exactly similar to gear-driven auxiliary supercharger operation, with the exception that the turbosupercharger tip-speed value is fixed regardless of the choice of engine speed.

A correction formula that applies to operation of a turbo-two-stage engine at altitudes below the turbo-critical altitude or critical turbo-speed is exceedingly complex and is therefore too cumbersome to use. This is because the operation and control of the turbo-stage is quite complicated. In attempting the derivation of the correction formula for "below-critical-altitude" use, it was assumed that the turbocontrol would be such as to maintain constant manifold pressure at the main stage supercharger-discharge annulus. For this reason, the correction will be termed the "constant-manifold-pressure" correction.

In order to simplify the correction formula as much as possible, it was also assumed that all corrections should be made at constant pressure altitude—i.e., $p_{as} = p_{ai}$. The constant manifold-pressure output correction formula, therefore, concerns the effects of changes of atmospheric air temperature on the turbo-engine output.

A brief explanation of the turbo-operation for changes in free-air temperature is deemed advisable to show its complexity.

Let it be assumed that the engine was tested in an atmospheric temperature somewhat above the standard value at the test pressure altitude. For this case the temperature at the entrance of both the primary and auxiliary stages would be in excess of the standard value, and the corresponding pressure rise ratio would be low in each supercharger unit. In order to obtain a definite manifold pressure, the turbowheel speed would be adjusted to a value somewhat higher than would be required if the atmospheric temperature were at its standard value.

A complicated relation for calculating the ratio of the turbowheel speeds under observed and standard conditions is as follows:

$$\frac{n_s}{n_i} = \frac{V_{1s}}{V_{1i}} = \left[\frac{T_{rs}}{T_{ri}Y_i}\left(\frac{p_{di}}{p_{ai}\left[1 + Y_{ri}\left(\frac{T_{ai}}{T_{as}}\right)\right]^{3.5}\left[1 + Y_i\left(\frac{T_{ci}}{T_{cs}}\right)^{1/2}\right]^{3.5}}\right.\right. \times$$

$$\left.\left.\frac{1}{\left[1 - \frac{p_{ci} - p_{bi}}{p_{ci}}\left(\frac{T_{ci}}{T_{cs}}\right)\right]\left[1 - \frac{p_{d1i} - p_{ci}}{p_{d1i}}\left(\frac{T_{d1i}}{T_{d1s}}\right)\right]}\right)^{0.283} - 1\right]^{1/s} \quad \text{(approx.)} \quad (66)$$

An unpredictable exhaust back-pressure change also accompanies the turbowheel speed change.

The approximate standard temperatures within the induction system at varying locations are given by Eqs. (29), (60), and the following equations:

$$T_{d1s} = (T_{d1i} - T_{ri})\left(\frac{V_{1s}}{V_{1i}}\right)^2 + T_{rs} \quad (67)$$

$$T_{cs} = T_{d1s}\left(\frac{T_{ci} - T_{ai}}{T_{d1i} - T_{ai}}\right) - T_{as}\left(\frac{T_{d1i} - T_{ci}}{T_{d1i} - T_{ai}}\right) \quad \text{(approx.)} \quad (68)$$

The combination of these relations gives an approximate formula for calculating the standard value of main-stage supercharger-discharge temperature:

$$T_{ds} = T_{di} - 0.812T_{ci} + 0.812\left[\left((T_{d1i} - T_{ri})\left(\frac{V_{1s}}{V_{1i}}\right)^2 + (T_{ri} - T_{ai} + T_{as})\right)\left(\frac{T_{ci} - T_{ai}}{T_{d1i} - T_{ai}}\right) - T_{as}\left(\frac{T_{d1i} - T_{ci}}{T_{d1i} - T_{ai}}\right)\right]^{1/2} \quad \text{(approx.)} \quad (69)$$

In the preceding equation the ratio V_{1s}/V_{1i} is given by Eq. (66). In order to obtain an actual final form of an equation for determining the standard value of main-stage supercharger-discharge temperature, the solution of some extremely complicated simultaneous equations is required. The relation of standard to observed horsepower would then be given by the relation

$$\text{b.hp.}_s = (\text{b.hp.}_i + \text{f.hp.}_i)(T_{di}/T_{ds}) - \text{f.hp.}_s \quad (70)$$

In view of the requirements of numerous assumptions and the complex nature of the derived basic equations, which involve many test measurements and unpredictable factors, it is believed that the presentation of a final formula for the constant manifold-pressure correction of turboengine output is unwarranted. Hence, none is included in this paper.

Conclusions

As a result of the analytic and experimental investigations of the problem of correcting engine output to standard conditions, it is concluded:

(1) That the commonly used full-throttle power

correction formula does not give accurate answers when applied to supercharged engine test data.

(2) That the commonly used part-throttle correction formula gives reasonably accurate answers when applied to single-stage engine test data.

(3) A rational full-throttle output correction formula for use with single-stage supercharged engines has been evolved and is presented as Eq. (35) in this paper. Experimental checks of this formula indicate that its accuracy is considerably better than the accuracy of the commonly used full-throttle power correction formula.

(4) A rational part-throttle output correction formula for use with single-stage supercharged engines has been evolved and is presented as Eq. (42) in this paper. Experimental checks of this formula indicate that its accuracy is inferior to that of the commonly used part-throttle correction formula.

(5) Rational full-throttle and part-throttle correction formulas are presented for use with two-stage engines of both the gear-driven and turbo-driven variety. For the direct gear-driven two-stage engine, Eqs. (64) and (65) are expected to give reasonably accurate results for full-throttle and part-throttle corrections, although no carefully controlled experiments are presented as proof of these formulas.

6. Output corrections for constant manifold-pressure operation of a turbosupercharged engine are so involved as to preclude the possibility of any accuracy of correction.

7. The full-throttle output-correction formula (Eq. 64) derived for the two-stage engine with gear-driven superchargers applies also to turbosupercharged engines, at altitudes above the critical altitude, where constant turbospeed is assumed.

REFERENCES

[1] Sparrow, Stanwood W., *Correcting Horsepower Measurements to a Standard Temperature*, N.A.C.A. Report No. 190, p. 125, 1925.

[2] Gove, W. D., *The Variation of Engine Power with Altitude Determined from Measurements in Flight with a Hub Dynamometer*, N.A.C.A. Report No. 295, p. 323, 1929.

[3] Dodge, Russell A., and Thompson, Milton J., *Fluid Mechanics*, 1st Edition, p. 221; McGraw-Hill Book Company, New York, 1937.

[4] Diehl, Walter S., *Standard Atmosphere—Tables and Data*, N.A.C.A. Report No. 218, p. 221, 1926.

[5] Zeyns, J., *The Air Consumption of Aircraft Engines at Altitude*, Deutsche Versuchsanstalt für Luftfahrt (Castleman Translation No. 120); Motor technischie Zeitschrift, pp. 145–151, November, 1939.

Letter to the Editor

Dear Sir:

The letter from W. K. Bodger in the March JOURNAL, commenting on the paper, "Determination of Strain Distribution by the Photo-Grid Process," is particularly gratifying to the authors, as it indicates an interest in the subject at an outstanding educational institution. It frequently occurs in industry that certain lines of research are limited to practical applications in that specific industry. When this point is reached it is of value to industry in general if the subject can be carried forward by a university or an institution having facilities for long-range research. The photo-grid process is being extensively used at Lockheed as a method of strain determination in a variety of forming operations, as described in "Elastic Theory Applied to Sheet Metal Forming," by F. R. Shanley.[1] However, a number of long-range projects utilizing the photo-grid system to study local deformation adjacent to cutouts and notches in both impact and static test specimens would be of value. Utilizing high-speed light sources it should be possible to measure the strain distribution over impact specimens similar to the diagram obtained at normal speed as shown in Fig. 1 of this paper, using a specimen similar to Fig. 2, reference 2.

Using the photo-grid process, finer grids may be placed over areas to be investigated in a fraction of the time required by a ruling engine. Furthermore, the deleterious effect of the scribed notch is not present. It would seem that the proper place for investigation into subjects similar to those suggested would be at a university, since the aircraft industry is at present preoccupied with the solution of immediate practical problems.

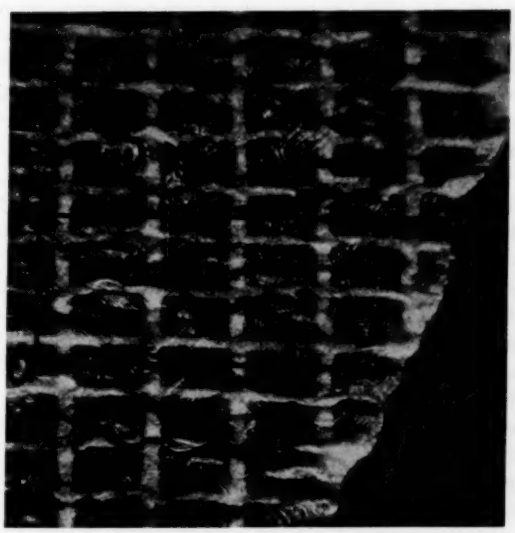

FIG. 1. Enlarged approximately 38 diameters.

Mr. Bodger has pointed out that true strain has been defined as

$$\epsilon = \int_{L_0}^{L} dL/L = \ln(L/L_0)$$

where L_0 equals the initial gauge length and L equals

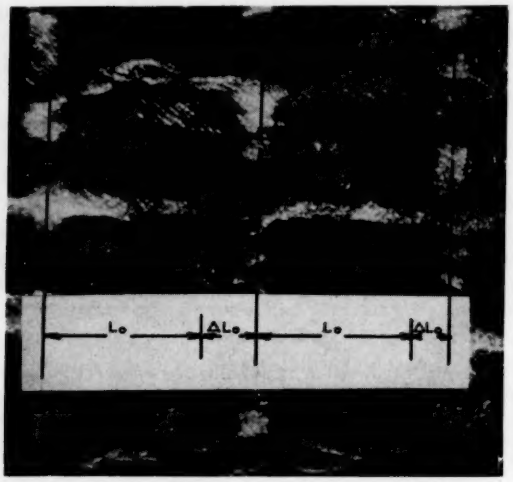

FIG. 2. Enlarged approximately 90 diameters.

the final gauge length (reference 3). In the same reference it has been shown that

$$\epsilon = \ln(L/L_0) = \ln(A/A_0)$$

Therefore, if the initial and final areas of the cross section are known, the true strain at that section may be calculated from the relationships given above. Mr. Bodger has suggested that the "hypothetical ultimate" strain referred to in our paper (reference 2, p. 4) was indeed the true strain at fracture; and that whereas we stated that this strain could only be determined by using a gauge length of differential size, actually this strain could be measured by the substitution of the measured initial and final areas into the relationship $\epsilon = \ln(A/A_0)$. Unfortunately, aircraft sheet materials necessarily involve material thicknesses that preclude the possibility of making round tensile specimens from the sheet, so that flat coupons following A.S.T.M. practice must be used. Utilizing the flat specimen it is difficult if not impossible to measure the final cross-sectional area of the jagged fracture zone and to decide which projection of this area is of significance. Furthermore, the "hypothetical ultimate" strain we referred to was considered to be $\epsilon_0 = \Delta L/L_0$ where L_0 was of differential size; this value would not be the true strain since the latter is

$$\epsilon = \int_{L_0}^{L} dL/L$$

according to definition, although it is a measure of the same quantity.

We have found that elongation tests are of use in the solution of practical forming problems when the values of strain determined over certain gauge lengths are applied to problems involving plastic deformation over gauge lengths of the same magnitude. Therefore, although $\epsilon_0 = \Delta L/L_0$ (or "engineering strain") differs greatly from the more classic definition of strain, the application of the former quantity to forming problems wherein the required deformations are also calculated as engineering strains is perfectly valid.

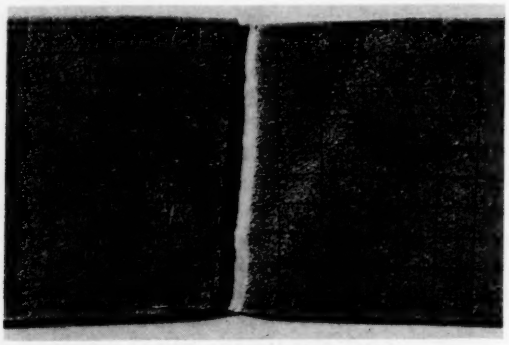

FIG. 3. Enlarged approximately 2 diameters, 0.1 in. line grid.

The use of true strain ϵ may be of value in translating stress-strain relationships in tension into stress-strain relationships under combined stress, such as those existing during the drawing process. However, as yet the full significance of the strain over a gauge length even as large as 0.01 in. has not been determined, so that the value of true strain or "ultimate" strain at the break is even more in question.

If the value of true strain at the fracture should later prove to be of importance in flat sheet metal, it might well be measured through the use of a photo grid of a size smaller than the average grain size of the metal in question and substituting L_0 (original grid spacing) and L (final grid spacing at fracture) into the true strain relationship. Referring to Fig. 2 of reference 2, the nonuniform nature of strain distribution along a specimen of polycrystalline material is clearly shown in the outlined zone. On such a specimen a grid utilizing a 0.04 in. gauge length would be much too coarse for an accurate determination of ϵ_0 or ϵ at the fracture; while a 0.01-in. grid would be reasonably accurate if we may assume that the grid is smaller than the average grain size and that the strain over a grain at the fracture zone is uniformly distributed. In this case, and in the case shown by Fig. 3, wherein a large Lüder line considerably alters the strain-distribution pattern, it would seem that the photo-grid process would offer a more valid method of determining the true strain than the reduction of area method.

REFERENCES

[1] Shanley, F. R., *Elastic Theory as a Tool in Sheet Metal Forming Problems*, Journal of the Aeronautical Sciences, Vol. 9, No. 9, pp. 313–333, July, 1942.

[2] Brewer, G., and Glassco, R. B., *Determination of Strain Distribution by the Photo-Grid Process*, Journal of the Aeronautical Sciences, Vol. 9, No. 1, pp. 1–7, November, 1941.

[3] MacGregor, C. W., "The Tension Test," Proc. A.S.T.M., Vol. 40, pp. 508–534, 1940.

G. A. BREWER
Senior Research Engineer
Lockheed Aircraft Corporation

A Theory for the Buckling of Thin Shells

HSUE-SHEN TSIEN*

California Institute of Technology

SUMMARY

In a series of papers written by the present author in collaboration with Th. von Kármán and Louis G. Dunn, the effect of curvature of a structure on its buckling characteristics was investigated. The purpose of these investigations was to find an explanation for the discrepancy between the "classic" theory and the experiments. For the case of a thin spherical shell under external pressure and for the case of a thin cylindric shell under axial compression, equilibrium states involving large deflections are discovered which can be maintained by loads far less than the so-called buckling load calculated by the classic theory of infinitesimal deflections. It was felt then that since some of these newly found equilibrium states closely approach the observed phenomena the shell must "jump" suddenly from the unbuckled configuration to these equilibrium states and the structures fail as a result of this sudden change. However, the reason why the shell should jump to these particular equilibrium states and not others was not explained. In the present paper a new principle involving the energy level and the geometric restraint is developed to determine this sudden change in equilibrium states. By means of this new principle the buckling load of both the spherical shell and cylindric shell can be calculated. The agreement with experiments is good.

INTRODUCTION

TOGETHER WITH THEODORE VON KÁRMÁN and Louis G. Dunn, the author[1, 2, 3] has suggested an explanation for the apparent discrepancy between the observed facts and the well-known classic theory for certain cases of the buckling of thin shells. The essential result of these investigations is the discovery of equilibrium states of the shell which involve a much lower applied load than the buckling load predicted by the classic theory. The load actually decreases as the deflection of the shell is increased. Some of the equilibrium states found are close to the experimentally observed ones both in the applied load and in the wave pattern. The authors then concluded that the unbuckled shell will suddenly jump to those equilibrium positions during the loading process without reaching the classic buckling load. However, the question why the shell should jump to these particular equilibrium states and not others remains to be answered. This is essentially the objection raised by K. O. Friedrichs[4] to the author's treatment of the buckling of spherical shells under external pressure. In the present paper the author will first try to clarify this point and then apply the theory to a number of special cases, for which experimental data are available, to test the validity of the theory. Finally, a more precise mathematical formulation of the buckling problem of spherical shells will be presented to indicate the possibilities of further investigations.

Presented at the Structures Session, Tenth Annual Meeting, I.Ae.S., New York, January 28, 1942.

* Research Fellow in Aeronautics.

THE CRITERIONS FOR BUCKLING

In the author's paper on cylindric shells under axial compression,[3] it is stated that under average laboratory and actual service conditions the most probable equilibrium state is the state with the lowest possible energy level. This statement is based upon the assumption that there are disturbances of sufficient magnitude so that the transitions from higher energy levels to lower energy levels are always possible. Although this assumption seems plausible, nevertheless it can only be verified by comparison with experiment. Since the available experimental data usually only give the buckling load of the specimen, the present investigation will be confined to buckling phenomena.

First of all the meaning of "possible energy levels," must be made clear. The two conditions for possible energy levels are: (1) the corresponding external forces and internal stresses must be in equilibrium; (2) the geometric restraint and loading conditions, if any, must be satisfied.

The second condition depends, of course, upon the manner in which the specimen is loaded. To facilitate the mathematical treatment, two limiting cases will be investigated first. If the specimen is loaded in axial compression, then one of these limiting loading processes is that of a rigid testing machine, and the other is that of "dead weight" loading.

In a testing machine the parameter over which the operator has direct control is the distance between the end plates, since this distance is determined by the position of the loading crank. The buckling of a thin shell usually occurs in a fraction of a second; therefore, the operator really has no time to turn the loading crank during the jump from the unbuckled state to the buckled state. In other words, the distance between the end plates is the same at the beginning and at the end of the buckling process. Hence, the geometric restraint in this case is the end shortening of the specimen. Thus, both the starting point of the jump and the end point of the jump must lie in a vertical line AB in the load vs. end-shortening diagram (Fig. 1). Since the end shortening of the specimen is constant, the potential energy of the loading force is not changed. The energy level of the system is given by the strain energy at a given value of the end shortening. Buckling will probably occur at a certain value of the end shortening which gives equal strain energy for both the

unbuckled equilibrium state and the buckled equilibrium state. If these two particular equilibrium states are presented by points A and B, respectively, the load of the specimen will jump from a higher value to a lower value corresponding to the distance between A and B. The load given by A which corresponds to the unbuckled equilibrium state is generally recorded as the failing load of the specimen.

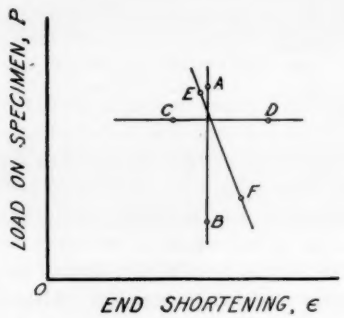

FIG. 1. Relation between the load and the end shortening for different types of loading processes.

In case of dead weight loading, the parameter under the control of operator is the amount of weight on the test specimen. However, he has no control of the end shortening of the test specimen which is determined by the equilibrium of the external force and the internal stresses. Hence, the starting point and the end point of the buckling process must lie on a horizontal line CD in the load vs. end-shortening diagram (Fig. 1). Because of the movement of the loading force during the buckling process, the potential energy of the loading weight must be included in calculating the energy level of the system. Thus, the energy level is given by the total potential Φ of the system,

$$\Phi = S - P\epsilon \tag{1}$$

where S is the strain energy, P the loading force and ϵ the end shortening of the specimen. Buckling will probably occur at a certain value of the load P which gives equal total potential Φ for both the unbuckled equilibrium state C and the buckled equilibrium state D. Therefore, referring to Fig. 1, the following relation exists

$$S_C - P\epsilon_C = S_D - P\epsilon_D \tag{2}$$

Or

$$S_D - S_C = P(\epsilon_D - \epsilon_C) \tag{3}$$

which means physically that the increase in strain energy of the specimen by jumping from the unbuckled to the buckled equilibrium states is provided by the decrease in potential energy of the load.

The limiting case of a perfectly rigid testing machine that will apply any load to the test specimen independent of the distance between the end plates really does not exist. In an actual testing machine there is always a certain amount of elasticity or "give." In other words, with the loading crank held fixed, the distance between the end plates will slightly increase if the load applied to the specimen is increased. Therefore, the starting point and end point of jumping of a specimen during buckling must lie on a straight line EF in Fig. 1, instead of the ideal case represented by the line AB. The more elastic the testing machine, the less will be the slope of the line EF. Therefore, the effect of the elasticity of the testing machine is to make the buckling phenomena more like that which would occur with dead weight loading. It will be shown later that the failing load of a specimen depends largely on the slope of the line EF. Hence, the elasticity of the testing machine has a strong influence on the failing load.

There are certain interesting relations connected with the important quantities, strain energy and total potential. Let the load P vs. end-shortening ϵ curve of a structure be given by Fig. 2. Then if the structure is brought up to the state P_1, ϵ_1, by following the equilibrium curve, the strain energy stored in the structure is certainly equal to the external work done by the loading force. Thus,

$$S(\epsilon_1) = \int_0^{\epsilon_1} P\epsilon d\epsilon \tag{4}$$

which is represented by the shaded area in Fig. 2a. The direction followed around the contour of this area is as indicated and is according to the usual convention. From Eq. (4) it is evident that

$$dS/d\epsilon = P \tag{5}$$

In other words, the slope of S vs. ϵ curve gives the load on the specimen.

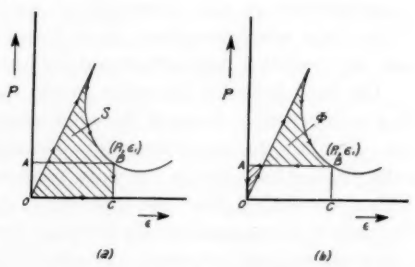

FIG. 2. Strain energy S and total potential Φ as integrals under the load P vs. end-shortening ϵ curve.

Using Eq. (1), the total potential Φ is given by the difference of the shaded area in Fig. 2a and the rectangle OABC. In other words, it can be calculated as the algebraic sum of the shaded areas in Fig. 2b. Consequently,

$$\Phi(P_1) = -\int_0^{P_1} \epsilon P dP \tag{6}$$

The integration is performed by following the contour as indicated in the figure. Eq. (6) can, of course, also

be obtained from Eq. (4) by partial integration. From Eq. (6), it is evident that

$$d\Phi/dP = -\epsilon \tag{7}$$

That is, the slope of Φ vs. P curve gives the end shortening of the specimen with a negative sign.

Both Eqs. (5) and (6) degenerate to rather trivial relations in case of linear load vs. end-shortening curves, but they are useful in nonlinear buckling problems. The relations between the quantities P and ϵ and the two potentials S and Φ are really equivalent to those existing between the pressure and volume and the internal energy and the heat content in thermodynamics.

Column with a Nonlinear Elastic Lateral Support

Using the results obtained in a previous investigation,[3] a preliminary calculation of the strain energy in a cylindric shell under axial compression shows that the relation between this quantity and the geometric restraint—i.e., the end shortening—is rather complicated. It is felt that since the method of calculating the equilibrium positions in this particular investigation is only an approximate one, the complicated relation between the strain energy and end shortening may not be very reliable. However, an exact solution of this problem is difficult. During the investigation of the general character of the buckling of shells[2] it was found that the characteristics of this type of structure can be very well simulated by a column (Fig. 3) supported laterally

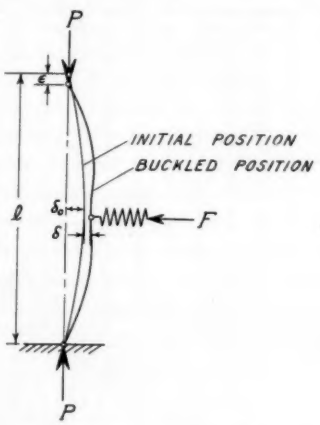

Fig. 3. Column supported laterally with a nonlinear spring.

by a spring whose load vs. deflection curve has a decreasing slope such as that shown in Fig. 4. This analogy was first suggested by H. L. Cox.[5] An exact solution of the column problem can be obtained without any mathematical difficulty.[6]

To test the validity of the theoretic analysis, the result of calculation is compared with experimental data. The experimental data were obtained from a column of 24RST of 0.090 in. thick by 0.375 in. wide and 19 in. long. The lateral support is a semicircular steel ring

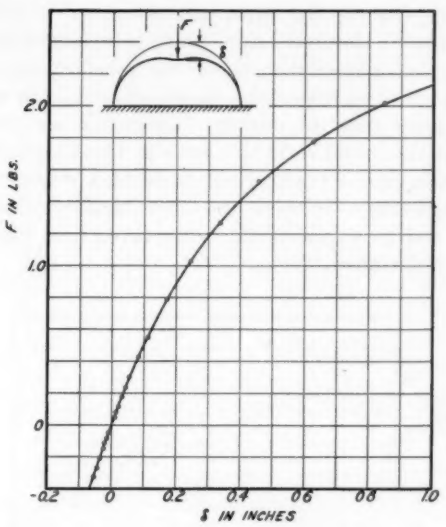

Fig. 4. Relation between the load F and the deflection δ for a semicircular ring.

0.015 in. thick by 0.50 in. wide. This steel ring gives a load F vs. deflection δ curve as indicated in Fig. 4. The columns were rolled to approximately a half sine wave. The amplitude of the initial deflection is denoted by δ_0. The test results are shown in Fig. 5 where $P_E = \pi^2 EI/l^2$ is the Euler column load, l is the length, I is the moment of inertia of the column section and E is Young's modulus of the material. The dotted line is the theoretic curve for a perfectly straight column using the supporting spring characteristics shown in

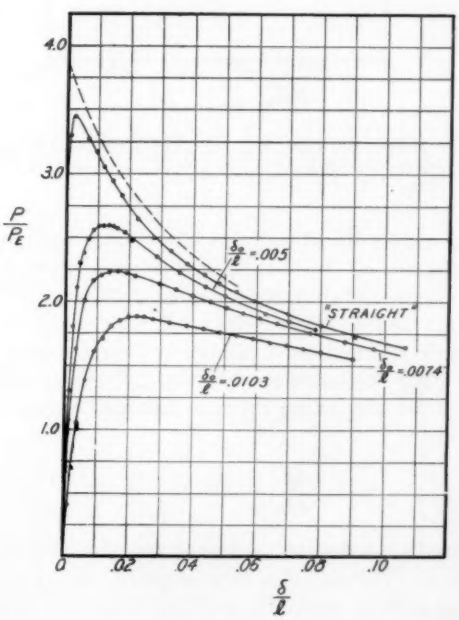

Fig. 5. Load P vs. deflection δ curves for columns supported laterally with a semicircular ring and with various amounts of initial deflection δ_0.

Fig. 4. One of the experimental curves is labeled "straight." However, it is practically impossible to obtain such a specimen; hence, the lower experimental values are to be expected. In Figs. 6 and 7 the maximum loads that the columns can sustain are plotted against the initial deflection ratio δ_0/l and against the deflection ratio δ/l at that maximum load, respectively. The agreement between the theoretically calculated curve and the experimental values taken from Fig. 5 is quite satisfactory.

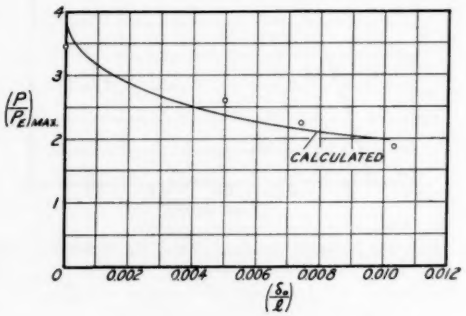

FIG. 6. Maximum load $P_{max.}$ as a function of initial deflection δ_0 for columns supported laterally with a semicircular ring.

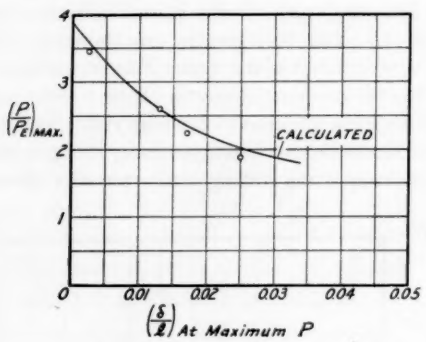

FIG. 7. Maximum load $P_{max.}$ as a function of deflection at the maximum load for columns supported laterally with a semicircular ring.

With this verification of the theory, a further investigation is carried out in which the relation between the strain energy and the end shortening of the column is the primary consideration. The end shortening is the geometric restraint for a column in a rigid testing machine. For this calculation the load F vs. deflection δ relation for supporting spring is assumed to be represented by

$$\frac{F}{P_E} = 13.712\,\frac{\delta}{l}\left(1 - 208.89\frac{\delta}{l} + 10444\frac{\delta^2}{l^2}\right) \qquad (8)$$

This load vs. deflection relation is similar to that shown in Fig. 4. The results of this calculation are presented in Figs. 8 and 9, where the end load ratio P/P_E and the strain energy S are plotted against the end shortening ϵ, respectively. In these figures i denotes the radius of

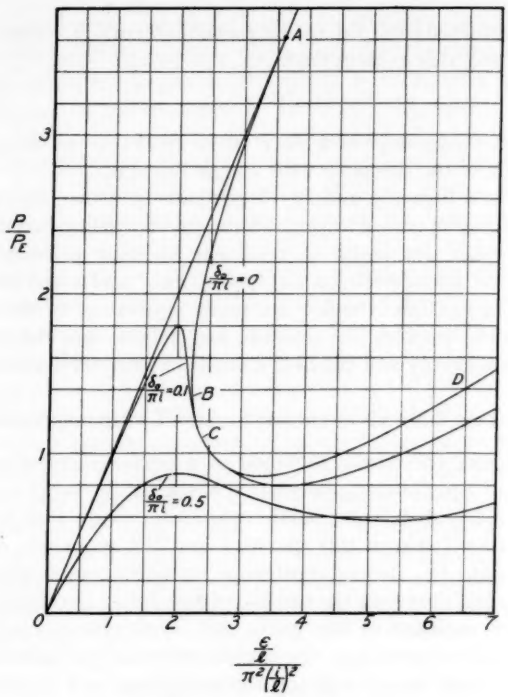

FIG. 8. Relation between the load P and the end shortening ϵ for columns with a nonlinear lateral support and various amounts of initial deflection δ_0.

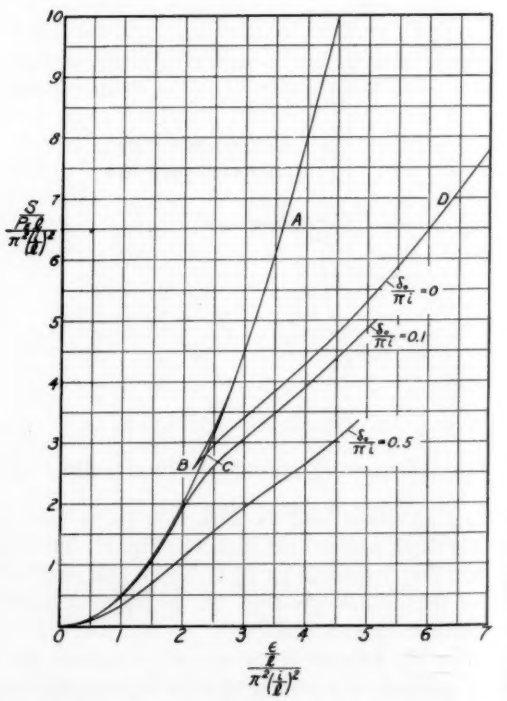

FIG. 9. Relation between the strain energy S and the end shortening ϵ for columns with a nonlinear lateral support and various amounts of initial deflection δ_0.

gyration of the column. For the case of a straight column, the load P/P_E first follows the straight line OA (Fig. 8) and then the curve AB. The point A represents the buckled state of the column with infinitesimal amplitude δ. All the other equilibrium positions in the buckled state involve finite amplitudes δ. Since the classic theory of buckling only considers infinitesimal displacement, the point A can be said to represent the classic buckling load.

In the strain energy diagram, Fig. 9, the corresponding points are denoted by the same letters as in Fig. 8. Thus, the straight equilibrium states of the column are represented by the parabola OA, and the buckled equilibrium states by the curve ABCD. It is interesting to notice that the curve AB closely follows the parabola OA—i.e., the strain energy is only slightly higher than that of straight column with the same end shortening. The curve turns sharply at B and meets the parabola at C. The branch CD has less strain energy for the same end shortening than either the straight column or the buckled state represented by AB. Therefore, according to the criterion of lowest strain energy, the actual behavior of the column in a testing machine when the end plates are gradually brought together will be, first, the straight unbuckled shape up to C. At C there will be a sudden change in the shape of the column to that which involves a finite amplitude δ and a jump in the magnitude of the load from $P/P_E = 2.40$ to $P/P_E = 1.09$. Since, according to Eq. (5), the slope of the S vs. ϵ curve is a measure of P/P_E, this jump in the magnitude of P/P_E is indicated in Fig. 8 by a sudden change in the slope of the two branches of the curve. From then on the column will behave according to the curve CD with increasing end shortening. Therefore, under ordinary conditions the classic buckling state does not appear in the buckling process at all, and the recorded failing load of the column will be $P = 2.40P_E$ instead of the classic value of $P = 3.61P_E$ corresponding to the point A.

The initial deflection δ_0 of the column tends first to decrease the failing load. Finally, the sudden jump in the value of P disappears completely when, at any given value of end shortening ϵ, there is only one value of the load P. For this particular problem the small initial deflection of $\delta_0 = 0.1\pi i$ is already big enough to eliminate the jump in the value of P (Figs. 8 and 9).

To investigate the behavior of the columns when loaded by weights, the total potential Φ has to be plotted against the load P. This is done in Fig. 10, using the same characteristics of the lateral support as given by Eq. (8). For the straight column, $\delta_0/\pi i = 0$, the unbuckled equilibrium states are represented by the parabola OC_0A_0. The classic buckling load is indicated by the point A_0. The curve $A_0B_0C_0$ represents the buckled equilibrium states. Using the buckling criterion developed in the previous sections, the column will maintain its unbuckled straight shape up to the point C_0 with $P/P_E = 1.196$, while the loading is gradually increased. At this value of P/P_E the column will suddenly jump from the unbuckled equilibrium state to the buckled equilibrium state. At the same time the value of the end shortening will change from $\epsilon/l = 1.19\pi^2(i/l)^2$ to $\epsilon/l = 5.60\pi^2(i/l)^2$. According to Eq. (7) this jump in the magnitude of the end shortening is signified in Fig. 10 by the sudden change in the slope of the two branches of the curve. Here, again, the failing load will be $P = 1.196P_E$ instead of the classic buckling load of $P = 3.61P_E$.

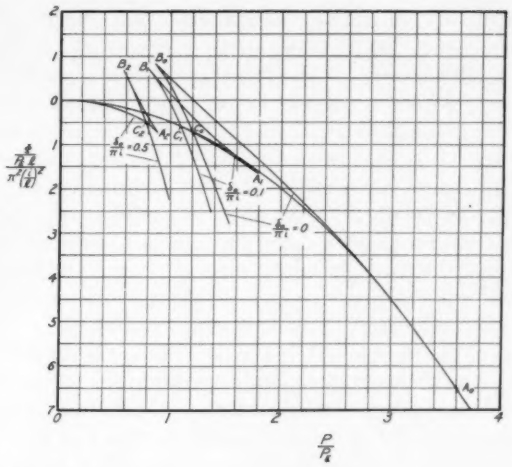

FIG. 10. Relation between the total potential Φ and the load P for columns with a nonlinear lateral support and various amounts of initial deflection δ_0.

The initial deflection δ_0 of the column again tends first to decrease the failing load. For $\delta_0/\pi i = 0.1$ the failing load is $P = 1.088P_E$; for $\delta_0/\pi i = 0.5$ the failing load is $P = 0.778P_E$. Finally, when at any given value of P there is only one equilibrium value of ϵ, the jump in the equilibrium states of the column during the loading process will disappear completely.

Summarizing the results, the failing load of a column with a nonlinear elastic support as given by Eq. (8) is given in Table 1. It is seen that under ordinary conditions the so-called classic buckling load really does not necessarily indicate the load carrying ability of the column.

TABLE 1

	P/P_E	—P/P_E of New Theory—	
$\delta_0/\pi i$	of Classic Theory	Testing machine	Dead weight
0	3.61	2.40	1.196
0.1	1.79	1.79	1.088
0.5	0.88	0.88	0.778

THIN UNIFORM CYLINDRIC SHELL UNDER AXIAL COMPRESSION

With the buckling criterions so clearly demonstrated by the failure of a column with nonlinear elastic sup-

port, the theory can now be applied with confidence to thin cylindric shells under axial compression. Using the results already obtained by the author in a previous paper,[3] the strain energy S of the shell and the total potential Φ can be calculated. The results are shown in Figs. 11 to 14. In these figures R is the radius, t is the thickness and ϵ is the unit end shortening of the shell. Furthermore, s denotes the strain energy per unit area of the shell surface, and φ is the total potential per unit area of the shell surface. The number of waves n in the circumference of the shell is determined by the parameter η which is equal to $n^2(t/R)$. The ratio of the wave length in the circumferential direction to that in the axial direction is defined as μ. Thus, for $\mu = 1$ the waves are square; for $\mu = 0.5$, the waves are rectangular with long side parallel to the axis of the cylindric shell. The value of Poisson's ratio is taken to be 0.3.

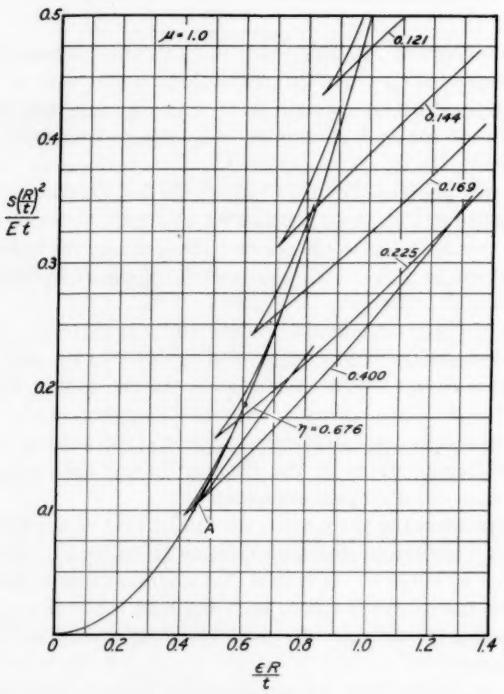

FIG. 11. Relation between the unit strain energy s and the unit end shortening ϵ for cylindric shells under axial compression with the aspect ratio μ of the waves equal to 1.0.

To investigate the behavior of the shell under a rigid testing machine, the strain energy parameter $s(R/t)^2/Et$ is plotted against the end-shortening parameter $\epsilon R/t$ as indicated in Figs. 11 and 12. According to the criterion developed in the previous sections, buckling will probably occur when the strain energy curve for the buckled equilibrium positions first crosses the curve for the unbuckled equilibrium positions. Thus, by referring to Fig. 11 for $\mu = 1.0$, the lowest probable buckling load is indicated by the point A. Then the corresponding

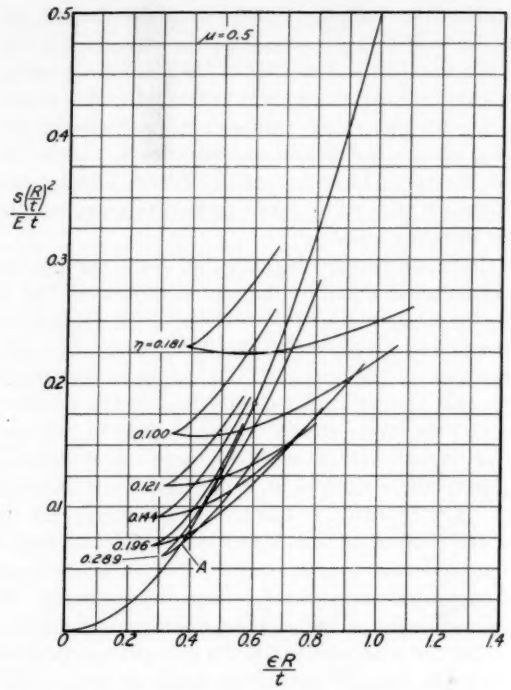

FIG. 12. Relation between the unit strain energy s and the unit end shortening ϵ for cylindric shells under axial compression with the aspect ratio μ of the waves equal to 0.5.

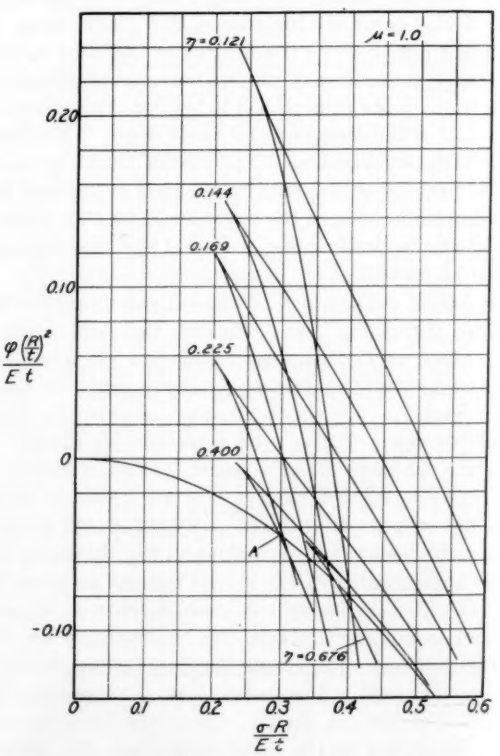

FIG. 13. Relation between the unit total potential φ and the compression stress σ for cylindric shells under axial compression with the aspect ratio μ of the waves equal to 1.0.

buckling load can be calculated as $\sigma R/Et = 0.460$ where σ is the average axial compression stress. The value of η is 0.400. Thus if $R/t = 1000$, $n = 20$. At buckling, the stress will jump from $\sigma = 0.460Et/R$ to $\sigma = 0.239Et/R$. With $\mu = 0.5$, Fig. 12 shows that the lowest probable buckling stress is around

$$\sigma = 0.370Et/R \tag{9}$$

The corresponding value of η is 0.289. Thus if $R/t = 1000$, $n = 17$. At buckling, the stress will jump from the value given by Eq. (9) to $\sigma = 0.2000Et/R$.

The failing load of the cylindric shell under dead weight loading can be determined from Figs. 13 and 14, where the total potential parameter $\varphi(R/t)^2/Et$ is plotted against the stress parameter $\sigma R/Et$ for $\mu = 1.0$ and $\mu = 0.5$, respectively. Using the criterion that buckling will probably occur for dead weight loading when the total potential curve for the buckled equilibrium state crosses the curve for the unbuckled equilibrium state. For $\mu = 1.0$, this happens at point A (Fig. 13), which corresponds to $\sigma = 0.298Et/R$. Again, since there is a sudden change in slope of the two branches of the curve which the shell will follow, the buckling phenomena is accompanied by a sudden increase in end shortening. By Fig. 14, for $\mu = 0.5$, the lowest probable buckling stress is around

$$\sigma = 0.238Et/R \tag{10}$$

Again, there will be a sudden change in the end shortening at buckling.

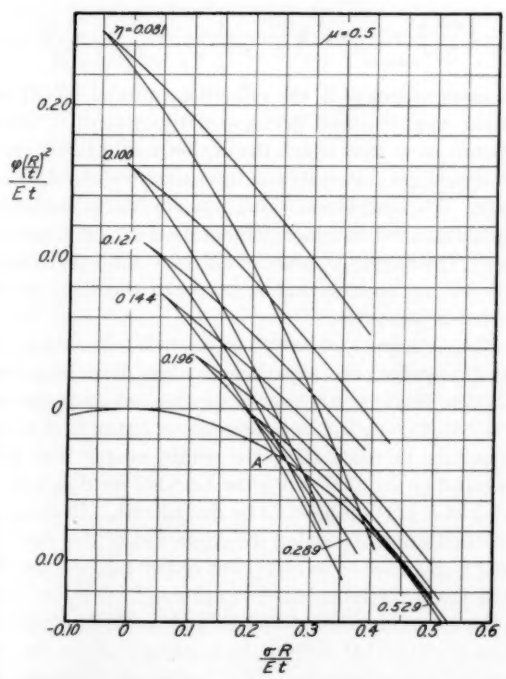

FIG. 14. Relation between the unit total potential φ and the compression stress σ for cylindric shells under axial compression with the aspect ratio μ of the waves equal to 0.5.

Both Eqs. (9) and (10) give a buckling stress much less than the classic buckling stress of $\sigma = 0.606Et/R$. As shown in the previous sections, the elasticity of the testing machine tends to lower the buckling stress toward that which would be obtained by dead weight loading. However, even the dead weight failing load given by Eq. (10) is higher than the average of the reported experimental data which give $\sigma = 0.15Et/R$.[2] One of the reasons for this failure of quantitative agreement between the theory and experiment is, of course, the approximate character of the method used in reference 3 which is the basis of the present calculation. Furthermore, the aspect ratio μ of the wave is chosen rather arbitrarily. There may well be other values of μ which will give lower values of the buckling stress. These questions can only be clarified by investigations to obtain more accurate solutions of the problem.

SPHERICAL SHELLS UNDER EXTERNAL PRESSURE

The buckling of thin uniform spherical shells under external pressure was investigated by the author in collaboration with Th. von Kármán[1] and by K. O. Friedrichs.[4] In the author's treatment there are several simplifying assumptions that were shown by Friedrichs to be unnecessary. Friedrichs, however, was unable to give a definite answer to the problem. Therefore, this problem will be treated now in the light of the present theory.

It was shown by Friedrichs that if the ratio of thickness to the radius of the shell and the angular extension of the buckle is small and if the additional radial and circumferential stresses due to buckling are zero at the boundary of the buckle then the difference between the sum of the additional strain energies of extension and bending and the virtual work of the external pressure force acting on the surface of the shell can be calculated by the following integral:

$$I = \frac{1}{2}\frac{(t/R)^2}{12(1-\nu^2)}\int_0^\beta \left(\frac{d\kappa}{d\alpha}\right)^2 \alpha^3 d\alpha + \frac{1}{2}\int_0^\beta \left[\int_\alpha^\beta \left(\kappa - \frac{1}{2}\kappa^2\right)\alpha d\alpha\right]^2 \alpha d\alpha - \frac{\sigma}{2E}\int_0^\beta \kappa^2\alpha^3 d\alpha \tag{11}$$

Here, t is the thickness, R is the radius of the spherical shell, β is the angular extension of buckle as shown in Fig. 15 and σ is the stress in the unbuckled shell under an external pressure p, and is equal to

$$\sigma = PR/2t \tag{12}$$

If, due to buckling, the inward radial displacement of the shell element is w, the function $\kappa(\alpha)$ is given by

$$\kappa(\alpha) = -(1/R\alpha)(dw/d\alpha) \tag{13}$$

To determine the equilibrium states the energy method can be used. For this purpose the radial displacement w is assumed to be

$$w/R = f[1 - (\alpha/\beta)^2]^2 \tag{14}$$

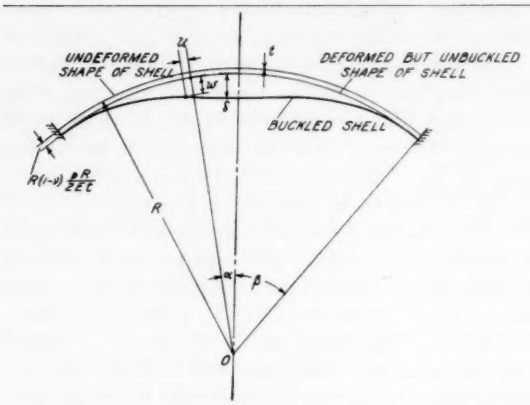

FIG. 15. Symmetric buckling of a spherical shell segment under external pressure.

where f is the ratio of the maximum radial displacement at the center of the buckle to the radius of the shell. This particular form of radial displacement has a zero slope at the boundary $\alpha = \beta$. However, the curvature is not zero at this boundary. Therefore, it requires a distribution of bending moment at the boundary to keep the buckled shell segment in equilibrium. Substituting Eq. (14) into Eq. (11), the integral I can be written as

$$I = \frac{4}{9}\frac{(t/R)^2}{(1-\nu^2)}\frac{f^2}{\beta^2} + \frac{\beta^2}{2}\left(\frac{1}{10}f^2 - \frac{2}{9}\frac{f^3}{\beta^2} + \frac{8}{63}\frac{f^4}{\beta^4}\right) - \frac{1}{3}f^2\frac{\sigma}{E} \tag{15}$$

To find the value of f at which the shell can be in equilibrium with a given value of σ, the derivative of I with respect to f has to be set equal to zero. Thus

$$\frac{\sigma}{E} = \frac{4}{3}\frac{(t/R)^2}{(1-\nu^2)}\frac{1}{\beta^2} + \beta^2\left(\frac{3}{20} - \frac{f}{2\beta^2} + \frac{8}{21}\frac{f^2}{\beta^4}\right) \tag{16}$$

Eq. (16) can be rewritten in a simpler form by using the following parameter:

$$\zeta = \beta^2 R/t, \quad \xi = fR/t \tag{17}$$

Then,

$$\frac{\sigma R}{Et} = \frac{4}{3}\frac{1}{(1-\nu^2)}\frac{1}{\zeta} + \frac{3}{20}\zeta - \frac{1}{2}\xi + \frac{8}{21}\frac{\xi^2}{\zeta} \tag{18}$$

When the amplitude of the buckle is very small, i.e., $\xi \to 0$, the minimum value of the buckling stress is given by

$$\sigma = 0.9376Et/R \tag{19}$$

with $\nu = 0.3$. This value is higher than the classic value

$$\sigma = 0.606Et/R \tag{20}$$

due to the special assumed deflection form given by Eq. (14). However, for the present calculation, the values of $\sigma R/Et$ for finite values of the amplitude ratio ξ are more interesting. Using Eq. (18), the value of $\sigma R/Et$ can be calculated as a function of ξ for various fixed values of ζ which determines the size of the buckle. The results are shown in Fig. 16.

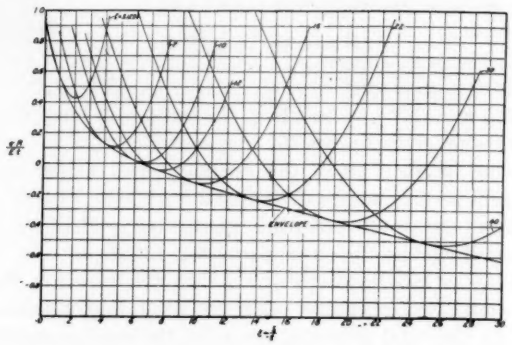

FIG. 16. Relation between the compression stress σ and the maximum deflection δ for a spherical shell segment under external pressure.

The envelope of curves shown in Fig. 16 can be obtained by differentiating Eq. (18) with respect to ζ and then setting the resultant expression equal to zero. Thus,

$$-\frac{4}{3}\frac{1}{(1-\nu^2)}\frac{1}{\zeta^2} + \frac{3}{20} - \frac{8}{21}\frac{\xi^2}{\zeta^2} = 0 \tag{21}$$

Combining Eqs. (21) with (18), the equation for the envelope curve is obtained as

$$\left(\frac{\sigma R}{Et}\right)_{Envelope} = \frac{1}{2}\sqrt{\frac{16}{5}\frac{1}{(1-\nu^2)} + \frac{32}{35}\xi^2} - \frac{1}{2}\xi \tag{22}$$

For large values of ξ, the envelope value of $\sigma R/Et$ will become negative and decrease without limit. This is different from that which the author found in his previous investigation[1] where a minimum value of $\sigma R/Et$ exists. This minimum value was due to the particular displacement of the shell element used in that investigation. The negative values of $\sigma R/Et$ at large deflections, however, are not the failing stress of the shell, as will be shown presently.

When a segment of a spherical shell is loaded by external pressure, the experiments show that in general only one single small buckle appears, whereas the rest of the shell remains in approximately spherical shape. Therefore, in calculating the strain energy and total potential of the shell, both the buckled portion and the unbuckled portion have to be considered. In the present calculation the radial displacement of the shell element is assumed to be composed of two parts: the uniform inward displacement equal to $(1-\nu)R\sigma/E$ due to the external pressure and an additional displacement given by Eq. (14) within the boundary of the buckled portion. Furthermore, the additional extensional stresses due to buckling are assumed to be zero at the boundary of the buckle. These assumptions result in

the following inaccuracies: (1) There is a discontinuity of curvature of the shell surface at the boundary of the buckle; (2) there is a discontinuity of the circumferential displacement of the shell elements at the boundary of the buckle; (3) the effective edge support at the boundary of the shell segment is neglected.

Since in all the calculations the ratio of the thickness to the radius of the shell is taken to be very small, it is probable that the errors introduced by the above-mentioned inaccuracies will not be appreciable.

With these assumptions, the strain energy s per unit area of the shell surface can be calculated by using Eq. (14) and expressions similar to Eq. (11). The result is

$$\frac{sR^2}{(1-\nu)t^3E} = \left(\frac{\sigma R}{Et}\right)^2 + \lambda\frac{t}{R}\frac{\zeta\xi}{(1-\nu)}\left[\frac{1}{3}\frac{\sigma R}{Et} + \left(\frac{4}{9(1-\nu^2)}\frac{1}{\zeta^2} + \frac{1}{20} - \frac{1}{3}\frac{\sigma R}{Et}\frac{1}{\zeta}\right)\xi - \frac{\xi^2}{9\zeta} + \frac{4}{63}\frac{\xi^3}{\zeta^2}\right] \quad (23)$$

where λ is the ratio of area of a hemisphere with radius R to the area of spherical segment. Therefore, if θ is the semiangular extension of the shell segment, λ can be written as

$$\lambda = 1/(1-\cos\theta) \quad (24)$$

If the shell is tested by means of external fluid pressure and the fluid is incompressible and enclosed in a chamber, the geometric restraint is the volume change of the shell due to its deflection. This volume change is caused by the uniform inward displacement due to the external pressure and the additional displacement given by Eq. (14) within the boundary of the buckled region. The change of volume v per unit area of the shell surface can be shown to be

$$\frac{v}{(1-\nu)t} = \frac{\sigma R}{Et} + \lambda\frac{(t/R)\zeta\xi}{6(1-\nu)} \quad (25)$$

This type of closed chamber fluid pressure test is equivalent to the so-called rigid testing machine test previously treated. From the similarity to the previously treated cases, the probable failing load of the shell is determined by the condition that the unbuckled and buckled equilibrium states have the same strain energy and same volume change. That is, if the quantities corresponding to the starting point of buckling are denoted by the subscript 1 and those corresponding to the end point of buckling by subscript 2, the conditions are

$$\zeta_1 = \xi_1 = 0 \quad (26)$$

$$\frac{\sigma_1 R}{Et} = \frac{\sigma_2 R}{Et} + \lambda\frac{t}{R}\frac{\zeta_2\xi_2}{6(1-\nu)} \quad (27)$$

$$\left(\frac{\sigma_1 R}{Et}\right)^2 = \left(\frac{\sigma_2 R}{Et}\right)^2 + \lambda\frac{t}{R}\frac{\zeta_2\xi_2}{(1-\nu)}\left\{\frac{1}{3}\frac{\sigma_2 R}{Et} + \left[\frac{4}{9(1-\nu^2)}\frac{1}{\zeta_2^2} + \frac{1}{20} - \frac{1}{3}\frac{\sigma_2 R}{Et}\frac{1}{\zeta_2}\right]\xi_2 - \frac{\xi_2^2}{9\zeta_2} + \frac{4}{63}\frac{\xi_2^3}{\zeta_2^2}\right\} \quad (28)$$

Eliminating σ_1 from Eqs. (27) and (28), the following relation is obtained.

$$\frac{4}{63}\frac{1}{\zeta_2^2}\xi_2^2 - \frac{1}{9\zeta_2}\xi_2 + \left[\frac{4}{9(1-\nu^2)}\frac{1}{\zeta_1^2} + \frac{1}{20} - \frac{1}{3}\frac{\sigma_2 R}{Et}\frac{1}{\zeta_2} - \frac{\lambda(t/R)\zeta_2}{36(1-\nu)}\right] = 0 \quad (29)$$

However, since at the end point of the buckling process the shell is at equilibrium, σ_2, ζ_2 and ξ_2 must also satisfy the equilibrium condition as given by Eq. (18). Thus,

$$\frac{8}{21}\frac{1}{\zeta_2}\xi_2^2 - \frac{1}{2}\xi_2 + \left[\frac{4}{3(1-\nu^2)}\frac{1}{\zeta_2} + \frac{3}{20}\zeta_2 - \frac{\sigma_2 R}{Et}\right] = 0 \quad (30)$$

Eqs. (29) and (30) give $\sigma_2 R/Et$ and ξ_2 as functions of ζ_2 for a given value of $\lambda t/R$. Then from Eq. (27) the expressions for $\sigma_1 R/Et$ and $\sigma_2 R/Et$ are,

$$\frac{\sigma_1 R}{Et} = \frac{4}{3(1-\nu^2)}\frac{1}{\zeta_2} + \frac{37}{480}\zeta_2 - \frac{3}{32}\frac{\lambda t/R}{(1-\nu)}\zeta_2^2 - \frac{\zeta_2}{24}\left[1 - \frac{\lambda t/R}{(1-\nu)}\zeta_2\right]\sqrt{\left(\frac{7}{4}\right)^2 - \frac{7\lambda t/R}{(1-\nu)}\zeta_2} \quad (31)$$

$$\frac{\sigma_2 R}{Et} = \frac{4}{3(1-\nu^2)}\frac{1}{\zeta_2} + \frac{37}{480}\zeta_2 - \frac{1}{6}\frac{\lambda t/R}{(1-\nu)}\zeta_2^2 - \frac{\zeta_2}{24}\sqrt{\left(\frac{7}{4}\right)^2 - \frac{7\lambda t/R}{(1-\nu)}\zeta_2} \quad (32)$$

and

$$\xi_2 = \zeta_2\left[\frac{7}{16} + \frac{1}{4}\sqrt{\left(\frac{7}{4}\right)^2 - \frac{7\,\lambda t/R}{(1-\nu)}\zeta_2}\right] \quad (33)$$

Fig. 17 indicates the calculated results for $\lambda t/R = 0.02101$. It is seen that as ζ_2 increases the value of $\sigma_1 R/Et$ first decreases and then increases again. The curves terminate at a value of ζ_2 which causes the expression under the radical in Eqs. (31), (32) and (33) to be equal to zero, because any further increase in ζ_2 will give imaginary values to the radical.

Since for a given shell segment only the value of $\lambda t/R$ is fixed, the size of the buckle or the parameter ζ_2 is free to vary, except that the size of the buckle cannot be larger than the size of the segment. Assuming for the moment that the last condition is not violated, then the actual probable failing load is determined by the minimum value of $\sigma_1 R/Et$. Denoting this minimum value by $\sigma_1{}^*R/Et$ and the corresponding $\sigma_2 R/Et$ by $\sigma_2{}^*R/Et$, then from Fig. 17, for $\lambda t/R = 0.02101$, $\sigma_1{}^*R/Et = 0.320$ and $\sigma_2{}^*R/Et = 0.125$.

By carrying out a series of computations for different values of $\lambda t/R$, $\sigma_1{}^*R/Et$ and $\sigma_2{}^*R/Et$ can be plotted against the parameter $R/t\lambda$. This is shown in Fig. 18. The upper curve which represents $\sigma_1{}^*R/Et$ then gives the failing load of the shell segment under the previ-

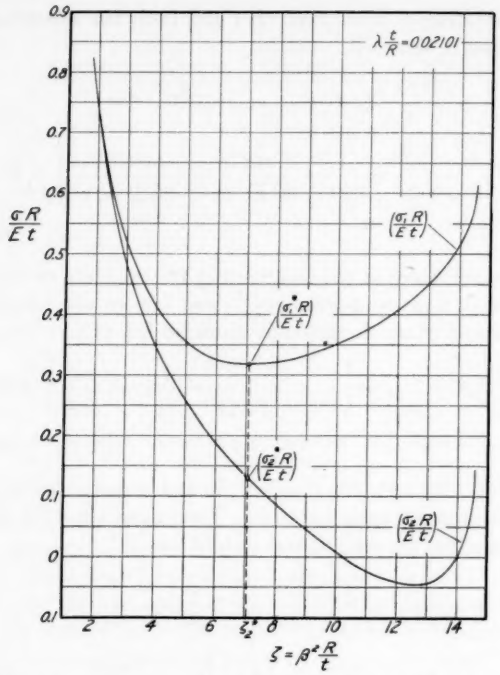

FIG. 17. Initial buckling stress σ_1 and final buckling stress σ_2 of a spherical shell segment under external pressure as a function of the angular extension β of the buckle.

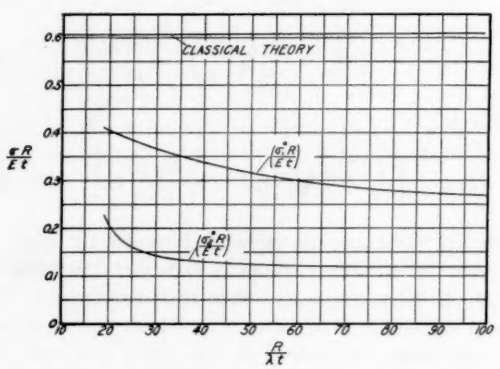

FIG. 18. Initial buckling stress σ_1^* and final buckling stress σ_2^* of spherical shell segments under external pressure.

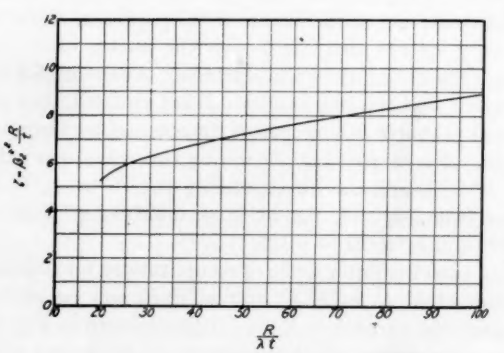

FIG. 19. Angular extension β_2^* of the buckle for spherical shell segments under external pressure.

ously stated conditions. This figure shows that the failing stress parameter $\sigma_1^* R/Et$ is no longer a constant as predicted by the classic theory but decreases slowly with increasing values of R/t if the solid angle of the segment—i.e., λ—is fixed. In fact, at a fixed value of λ it is found that

$$\sigma_1^*/E \sim (t/R)^{1.25} \tag{34}$$

for $20 < R/\lambda t < 100$. Furthermore, as shown in Fig. 19, the value of ζ_2^* at which $\sigma_1^* R/Et$ occurs also decreases with increasing R/t. It is found that with a fixed value of λ within the range stated ζ_2^* varies approximately as $(R/t)^{0.28}$. Then, according to Eq. (17), β_2^* varies approximately as $(R/t)^{-0.36}$. However, if l is the diameter or wave length of the buckle, $l/2R = \beta_2^*$. Then

$$l/t \sim (t/R)^{-0.64} \tag{35}$$

The exponents of t/R for a buckling stress σ/E and a wave length l/R given by the classic theory are, of course, 1 and $-1/2$, respectively.

There is no experiment known to the author which is performed under the geometric restraint that the enclosed volume of the shell during the buckling must be constant. However, a number of experiments have been conducted at the California Institute of Technology on clamped spherical shell segments of $\theta = 17$ deg. 45 min. subjected to water pressure.† The water is slowly admitted to a closed chamber whose top cover is the shell segment. The water is immediately turned off as soon as the shell starts to buckle, so that the volume of water in the chamber is nearly constant during the buckling process. However, the pressure of the water is measured by a mercury manometer connected to the chamber by a piece of rubber tubing which is filled with air at the beginning of the test. Both the drop in height of the mercury column and the expansion of air trapped in the rubber tubing will effectively increase the volume of the chamber. Therefore, these tests are somewhat similar to that of a column loaded in a partially elastic testing machine. The results of these tests are shown in Fig. 20 where the values of $\sigma R/Et$ for the beginning of buckling and the end point of buckling are plotted against (R/t). It is seen that both values tend to drop off slightly as R/t increases, which is a feature also shown by the theoretic calculation for constant volume restraint. The dotted curves represent $\sigma_1^* R/Et$ and $\sigma_2^* R/Et$ previously calculated. Although the test points do follow the curves very well, the agreement can only be regarded as qualitative because of the difference in the test conditions of these two cases.

If the shell segment is loaded by means of fluid pressure and the fluid is drawn from a large reservoir with a free surface, then the small change of volume during the

† The experiments were carried out by Mr. H. B. Crockett under Dr. L. G. Dunn's supervision. The author is deeply grateful to both of them.

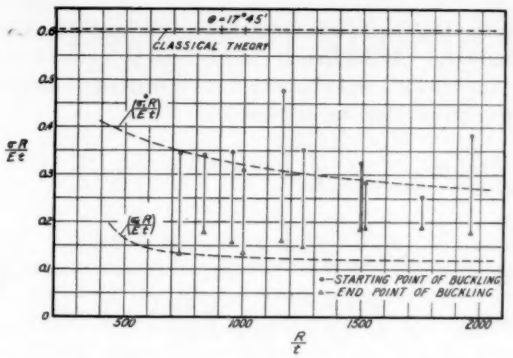

FIG. 20. Initial buckling stress and final buckling stress of spherical shell segments loaded with water pressure (experiments).

buckling process will not appreciably change the level of the fluid in the reservoir. Under such test conditions, the pressure acting on the shell at the starting point of buckling is practically the same as that at the end point of buckling. Let the volume change be ΔV: then the corresponding work done by the fluid is given by $p\Delta V$. This amount of work done must be equal to the increase in strain energy of the shell. This will give a similar relation as Eq. (3). Therefore, if the total potential Φ of the system is defined as

$$\Phi = S - pV \tag{36}$$

the buckling will occur when, at equal values of $\sigma R/Et$, the total potential of the unbuckled equilibrium state is the same as that of the buckled equilibrium state. By means of Eqs. (36), (23) and (25), the total potential φ per unit area of the shell surface can be expressed as

$$\frac{\varphi R^2}{(1-\nu)t^3E} = -\left(\frac{\sigma R}{Et}\right)^2 + \lambda\frac{t}{R}\frac{\zeta\xi^2}{(1-\nu)} \times \left\{\left[\frac{4}{9(1-\nu^2)}\frac{1}{\zeta^2} + \frac{1}{20} - \frac{1}{3}\frac{\sigma R}{Et}\frac{1}{\zeta}\right] - \frac{\xi}{9\zeta} + \frac{4}{63}\frac{\xi^2}{\zeta^2}\right\} \tag{37}$$

Let $\sigma_3 R/Et$ be the buckling stress parameter for this type of loading; then the buckling criterion stated above requires that

$$-\left(\frac{\sigma_3 R}{Et}\right)^2 = -\left(\frac{\sigma_3 R}{Et}\right)^2 + \lambda\frac{t}{R}\frac{\zeta_3\xi_3^2}{(1-\nu)} \times \left\{\left[\frac{4}{9(1-\nu^2)}\frac{1}{\zeta_3^2} + \frac{1}{20} - \frac{1}{3}\frac{\sigma_3 R}{Et}\frac{1}{\zeta_3}\right] - \frac{\xi_3}{9\zeta_3} + \frac{4}{63}\frac{\xi_3^2}{\zeta_3^2}\right\} \tag{38}$$

Thus,

$$\frac{4}{63}\frac{1}{\zeta_3^2}\xi_3^2 - \frac{1}{9}\frac{\xi_3}{\zeta_3} + \left[\frac{4}{9(1-\nu^2)}\frac{1}{\zeta_3^2} + \frac{1}{20} - \frac{1}{3}\frac{\sigma_3 R}{Et}\frac{1}{\zeta_3}\right] = 0 \tag{39}$$

On the other hand, since the buckled shell must be in equilibrium, Eq. (18) must also be satisfied. Therefore,

$$\frac{8}{21}\frac{1}{\zeta_3}\xi_3^2 - \frac{1}{2}\xi_3 + \left[\frac{4}{3(1-\nu^2)}\frac{1}{\zeta_3} + \frac{3}{20}\zeta_3 - \frac{\sigma_3 R}{Et}\right] = 0 \tag{40}$$

From Eqs. (39) and (40) $\sigma_3 R/Et$ and ξ_3 can be obtained as functions of ζ_3. Then,

$$\frac{\sigma_3 R}{Et} = \frac{1}{240}\zeta_3 + \frac{4}{3(1-\nu^2)}\frac{1}{\zeta_3} \tag{41}$$

and

$$\xi_3 = (7/8)\zeta_3 \tag{42}$$

If the shell segment is large enough, the actual buckling load will be determined by the minimum of $\sigma_3 R/Et$. Denoting quantities corresponding to this minimum by an asterisk, calculations show that

$$\sigma_3{}^* R/Et = 1/3\sqrt{5(1-\nu^2)} \tag{43}$$

$$\zeta_3{}^* = 8\sqrt{5/(1-\nu^2)} \tag{44}$$

and

$$\xi_3{}^* = 7\sqrt{5/(1-\nu^2)} \tag{45}$$

It should be noted that under this type of testing the buckling stress parameter $\sigma_3{}^* R/Et$ is again a constant as in the classic theory. However, the numerical value of this constant is only about one-fourth of the classic value.

The experiment on a hemispherical shell made by E. E. Sechler and W. Bollay was performed by immersing the shell in a mercury bath. Hence, the test conditions approximate the constant pressure type to which Eqs. (43), (44) and (45) applies. In Table 2 the values predicted by Eqs. (43), (44) and (45) are compared with those deduced from the test. The agreement between theory and experiment is truly remarkable.

TABLE 2

	Experiment	Theory
$\sigma_3 R/Et$	0.154	0.1561
$B_3{}^*$	8 deg.	8.3 deg.
$\xi_3{}^* = \delta^*/t$	12.5	16.4

CONCLUDING REMARKS

In the previous sections a new principle for determining the buckling load of curved shell under ordinary test and service conditions has been developed. This principle of lowest energy level is verified by comparing the experimental data with the theoretic predictions. However, in view of the prerequisite that arbitrary disturbances of finite magnitude have to exist, the buckling load determined by this principle may be called the "lower buckling load." The classic buckling load that assumes only the existence of disturbances of infinitesimal magnitude may be called the "upper buckling

load." Of course, by extreme care in avoiding all disturbances during the test, the upper buckling load can be approached. The lower buckling load, however, has to be used as the correct basis for design.

It may well be mentioned here that the possibility of the existence of the lower buckling load is connected with the elastic characteristics of the structure—i.e., the load on the structure must decrease as the deflection is increased. If this is not the case, the lower buckling load does not occur, and the buckling load of the structure can be closely calculated by the classic theory, as shown by the well-known case of a flat plate under edge compression. The author believes that when a cylindric shell is loaded by external lateral pressure, the load rises with the increase in the deflection of the shell surface after buckling. Therefore, for this case, also, the buckling load can be closely predicted by means of the classic theory of thin shells.[7]

To indicate the possible future developments, the problem of buckling of a spherical shell of constant thickness under uniform dead weight pressures will be formulated more precisely. If the radial and circumferential displacements of the median surface of the shell from its spherical equilibrium positions are denoted by w and u, respectively, the strains and change in curvatures can be calculated as[4]

$$\epsilon_r = \frac{(du/d\alpha) - w}{R} + \frac{1}{2}\frac{[(dw/d\alpha) + u]^2}{R^2}$$

$$\epsilon_c = (u \cot \alpha - w)/R$$

$$\chi_r = \frac{(d^2w/d\alpha^2) + w}{R^2} - \frac{1}{2}\frac{[(dw/d\alpha) + u]^2}{R^3} \qquad (46)$$

$$\chi_c = \frac{(dw/d\alpha)\cot\alpha + w}{R^2}$$

α is the angle between the radius vector and the axis of symmetry. The difference in the total potential $\Phi - \Phi_0$ for the buckled and unbuckled state with same external pressure can then be expressed as

$$\frac{\Phi - \Phi_0}{\pi R^2 Et} = \frac{1}{(1-\nu^2)}\int_0^\pi \left(\epsilon_r^2 + \epsilon_c^2 + 2\nu\epsilon_r\epsilon_c\right) \sin\alpha d\alpha + \frac{t^2}{12(1-\nu^2)}\int_0^\pi (\chi_c^2 + \chi_r^2 + 2\nu\chi_c\chi_r \qquad (47)$$

$$\sin\alpha d\alpha - \frac{\sigma}{E}\int_0^\pi \left[\left(1 + \frac{1}{12}\frac{t^2}{R^2}\right)\left(\frac{dw}{d\alpha} + u\right)^2 \Big/ R^2 - \frac{t^3}{3R^2}\frac{w}{R} + \frac{4w}{R}\left(\frac{1}{R}\frac{du}{d\alpha} + \frac{u}{R}\cot\alpha\right) - 4\frac{w^2}{R^2} - 8(1-\nu)\frac{\sigma}{E}\frac{w}{R}\right] \sin\alpha d\alpha$$

All equilibrium positions can be determined by the condition that the variations of the integral with respect to w and u must be zero. Or

$$\delta[(\Phi - \Phi_0/\pi R^2 Et)]_w = 0 \qquad (48)$$

$$\delta[(\Phi - \Phi_0/\pi R^2 Et)]_u = 0$$

The upper buckling load is determined by the additional condition that

$$w = u \to 0 \qquad (49)$$

The lower buckling load is determined by the additional condition that

$$(\Phi - \Phi_0)/\pi R^2 Et = 0 \qquad (50)$$

The problem of determining the lower buckling load thus becomes a special case of the well-known isometric problem in variational calculus.

References

[1] von Kármán, Th., and Tsien, Hsue-Shen, *The Buckling of Spherical Shells by External Pressure*, Journal of the Aeronautical Sciences, Vol. 7, No. 2, pp. 43–50, December, 1939.

[2] von Kármán, Th., Dunn, Louis G., and Tsien, Hsue-Shen, *The Influence of Curvature on the Buckling Characteristics of Structures*, Journal of the Aeronautical Sciences, Vol. 7, No. 7, pp. 276–289, May, 1940.

[3] von Kármán, Th., and Tsien, Hsue-Shen, *The Buckling of Thin Cylindrical Shells Under Axial Compression*, Journal of the Aeronautical Sciences, Vol. 8, No. 8, pp. 303–312, June, 1941.

[4] Friedrichs, K. O., *On the Minimum Buckling Load for Spherical Shells*, Theodore von Kármán Anniversary Volume, pp. 258–272, California Institute of Technology, Pasadena, 1941.

[5] Cox, H. L., *Stress Analysis of Thin Metal Construction*, Journal of the Royal Aeronautical Society, Vol. 44, No. 351, pp. 231–282, March, 1940.

[6] Tsien, Hsue-Shen, *Buckling of a Column with Non-Linear Lateral Supports*, Journal of the Aeronautical Sciences, Vol. 9, No. 4, pp. 119–132, February, 1942.

[7] A review of the theoretic investigations made by Lorentz, R., Southwell, R. V., and Mises, R. v., together with references is given in: Timoshenko, S., *Theory of Elastic Stability*, pp. 445–453, McGraw-Hill, New York, 1936. The comparison between the theory and the experiments is given by: Saunders, H. E., and Windenburg, D. F., *Strength of Thin Cylindrical Shells Under External Pressures*, Trans. A.S.M.E., Vol. 53, pp. 207–218, 1931.

Tricycle Landing Gear Design—Part 1*

E. S. JENKINS† AND A. F. DONOVAN‡
Curtiss-Wright Corporation

ABSTRACT

THE PROBLEMS OF THE tricycle landing gear are discussed in the light of available information with the object of providing criteria to assist the designer. The general geometric arrangement involving the determination of wheel base, tread, and center of gravity location is first considered. It is shown that the nose wheel should be located as far forward of the center of gravity as possible, and that the fore-and-aft location of the rear wheels is limited to a narrow range by conditions of balance and longitudinal stability. The relationship between tread, wheel base, and the resistance to turning over is found, and the effects of tread and fore-and-aft location of the rear wheels on the directional stability and ground maneuverability are discussed.

The problems related specifically to the design of the nose wheel are next examined, and a basis for the selection of nose wheel and tire size is given. The fundamental causes of shimmy are reviewed, including the effects of trail, caster angle, wheel offset, tire type, and moment of inertia of castering parts. Shimmy elimination is discussed with special reference to elimination by damping and including methods of calculating the amount of damping necessary to prevent shimmy. The construction of fluid dampeners is described, and their damping characteristics are compared to the simpler mathematically defined types of damping. An empirical relationship between the volume of a vane-type hydraulic dampener necessary to prevent shimmy and the static nose wheel load is given.

Ground handling and maneuverability, construction and installation difficulties, castering locks and stops, and steering devices are briefly discussed. Conclusions as to the best arrangements must be based on the characteristics of the particular design. As a partial check on the validity of the criteria developed, the results of applying them to some successful tricycle gear airplanes are summarized.

INTRODUCTION

The susceptibility of the conventional tail wheel landing gear to nosing over, its inherent tendency to ground loop (particularly in a side wind), and the necessity of making a full-stall landing to prevent bouncing have made it less and less satisfactory as landing speeds increased. The tricycle landing gear will eliminate these undesirable characteristics if properly designed, but it may introduce other objectionable features peculiar to its type. Some of these possible difficulties are porpoising, longitudinal instability with the nose wheel off the ground, shimmy of the nose wheel, and failure of the nose wheel strut from excessive dynamic loads. In addition, it should be remembered that the very fact that the faults of the conventional gear are eliminated will result in increased loads on the structure. Removal of the possibility of nosing over will lead to faster taxiing and use of full power on muddy fields, elimination of the ground-loop tendency will result in more cross-wind landings, and the lack of any tendency to bounce will mean more landings at high sinking speeds.

Many investigations, both theoretic and experimental, have been made of tricycle gear characteristics. Most of these, however, are either of a rather general nature or do not present their results in a manner that may be easily used in design work. Frequently, the conclusions reached are erroneous as a result of simplifying assumptions that ignore important factors. Even design criteria of the various authorities are sometimes unreliable since they are usually only an adaptation of the conventional gear criteria to the geometry of the tricycle type or have not been revised in the light of practical experience.

This paper is an attempt to provide reliable information on the tricycle gear obtained from both the literature on the subject and independent investigations. Considerable attention has been given to presenting the information in a manner to permit the quick solution of the various design problems. Most of the results are presented graphically in a series of charts which may be applied directly in the majority of cases. The paper is separated into two major divisions. Part 1 deals with the general geometry of the gear, such as the wheel base, tread, and location relative to the airplane. Part 2 is concerned with the nose wheel design and considers the problems of nose wheel size, trail, caster angle, and shimmy dampeners.

Presented at the Design Session, Tenth Annual Meeting, I.Ae.S., New York, January 29, 1942.

Copyright, 1942, by E. S. Jenkins and A. F. Donovan.

* Because of the length of this article it will be published in two parts. Part 2 dealing with Nose Wheel Design will be published in the September issue.

† Division Chief, Materials and Structures Research.
‡ Research Engineer.

General Geometry

Wheel Base

General

The effect of wheel base on the characteristics of the landing gear cannot be determined without consideration of its locations relative to the center of gravity and mean aerodynamic center of the airplane. The analysis becomes much simpler if instead of considering the effect of wheel base as a whole it is broken down into the effect of the horizontal distances of the front and rear wheels from the c.g. and the distance of the rear wheels aft of the aerodynamic center.

Nose Wheel Location

The principal item affected by the distance of the nose wheel forward of the c.g. is the nose wheel load. Other characteristics related to this dimension are the stability against overturning and the resistance to porpoising.

In attempting to find the landing loads on the nose wheel, some consideration must be given to the possible landing attitudes of the airplane. The three principal landing modes for a tricycle gear type may be defined as three-wheel landing, rear wheels first landing, and nose wheel first landing. In the three-wheel landing, the load distribution between the front and rear wheels is usually assumed to be the same as the static distribution. Actually, the shock absorber characteristics may result in a distribution considerably different from the static. By the conventional assumption, however, the nose wheel load in a three-wheel landing is

$$P_N = nW(l - l_1)/l \tag{1}$$

where l is the wheel base; l_1, the horizontal arm from the c. g. to the nose wheel; n, the acceleration; and W, the airplane weight.

In a rear wheels first landing, the proximity of the rear wheels to the c.g. will result in most of the energy being absorbed there, after which the airplane will drop over on the nose wheel. The nose wheel load from this condition may therefore be expected to be less than in the three-wheel landing.

In a nose wheel first landing, the nose wheel striking the ground tends to rotate the airplane. The load on the nose wheel thus depends on the pitching moment of inertia of the airplane. This load can be determined in terms of the acceleration at the nose wheel. The acceleration at the nose wheel may be found, in turn, from the shock absorber travel and airplane sinking speed.

Let

l_1 = horizontal distance from the nose wheel to the c.g.
W = airplane weight
W/g = airplane mass
g = acceleration of gravity
k = airplane pitching radius of gyration
a = vertical acceleration at airplane c.g.
a_N = vertical acceleration of the airplane at the nose wheel
ω = angular acceleration of airplane

If the airplane strikes the ground on the nose wheel with a force, F, the torque about the c.g. is Fl_1 and the angular acceleration is the torque divided by the pitching moment of inertia or

$$\omega = Fl_1/k^2(W/g) \tag{2}$$

The acceleration at the c.g. produces the force F, or

$$F = Ma = (W/g)a \tag{3}$$

The acceleration of a point on the airplane above the nose wheel is equal to the acceleration at the c.g. plus the effect of the angular acceleration. The angular acceleration has a vertical component at the nose wheel of ωl_1. The total vertical acceleration of the airplane at the nose wheel is therefore

$$a_N = a + \omega l_1 \tag{4}$$

Substituting Eq. (1) in Eq. (2)

$$a_N = a + [Fl_1^2/k^2(W/g)]$$

Replacing F by Eq. (3)

$$a_N = a + (W/g)al_1^2/(W/g)k^2$$

or

$$a_N = a[1 + (l_1^2/k^2)]$$

Therefore

$$a = a_N[k^2/(k^2 + l_1^2)] \tag{5}$$

The acceleration at the airplane c.g. is thus always less than at the nose wheel except when l_1 becomes zero or what amounts to the same thing if the nose wheel were put at the c.g. In this special case, of course, the acceleration at the nose wheel becomes the same as the acceleration at the c.g.

The load on the nose wheel, F, can now be found by use of Eq. (3).

$$F = (W/g)a = (W/g)a_N[k^2/(k^2 + l_1^2)] \tag{6}$$

If the acceleration is given in terms of gravity, the term a_N/g can be replaced by n_N

$$F = Wn_N[k^2/(k^2 + l_1^2)] \tag{7}$$

The acceleration, n_N, acting on the airplane at the nose wheel is determined by the vertical velocity at which the airplane strikes the ground and the characteristics of the nose wheel shock absorber. The value of n_N can be determined by a drop test of the nose wheel assembly from a height that will give the desired sinking

speed at the time of impact with an equivalent weight on the nose wheel of

$$w = W[k^2/(k^2 + l_1^2)] \tag{8}$$

The load factor determined from this drop test is n_N and must not exceed the design load factor for the nose wheel and supporting structure. If the nose wheel travel and the sinking speed are the same as that of the main gear, the load factor n_N will be approximately the same as that of the main gear in the three-wheel landing condition. Should the nose wheel travel be different from that of the rear wheels, the nose wheel load factor would be affected approximately in the inverse ratio of the wheel strokes. As the nose wheel travel is usually the same as the main wheels and as the same sinking speed is usually assumed for all conditions, the load on the nose wheel in a nose wheel first landing may be taken as

$$P_N = nW[k^2/(k^2 + l_1^2)] \tag{9}$$

where n is the load factor for a three-wheel landing.

From Eq. (9) it is apparent that, unlike the three-wheel landing where the nose wheel load is expressed by Eq. (1), the total wheel base has no effect on the front wheel reaction. The term nW appears in both equations, but the percentage of nW acting on the nose wheel is determined by entirely different factors. In the three-wheel landing, the distribution, being done by simple statics, is easily understood. The meaning of the expression $k^2/(k^2 + l_1^2)$ in Eq. (5) through Eq. (9) is not so easily recognized. A simple analogy will help explain its significance.

The terms in Eq. (1) are unaffected by the distribution of the items comprising the weight, W, with respect to the c.g. so long as the c.g. remains at the same point. Thus, if the engine were taken out of the nose of an airplane and put near the c.g. position and the radiators and some other equipment were taken from the tail and moved far enough forward to balance the airplane at the original c.g. position, the nose wheel load as determined by Eq. (1) for a three-wheel landing would remain the same. The load for a one-wheel landing would be markedly reduced, however, because the shift of the masses making up the airplane would have reduced k^2. Thus, although the c.g. and the weight remained the same, the nose wheel load was reduced. With the engine in the nose immediately above the nose wheel, the engine inertia had to be absorbed by the nose wheel. Moving the engine back in the airplane left the engine practically free to continue falling when the nose wheel hit and thus largely relieved the nose wheel of decelerating the engine. It is possible to represent the airplane by an arrangement of two concentrated masses that will produce the same loads on the landing gear. In this equivalent airplane (Fig. 1) the weight is divided so that a concentrated weight equal to Eq. (8) is located directly over the nose wheel. The remainder of the weight $(W - w)$ is concentrated

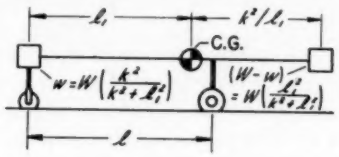

FIG. 1. Equivalent weight distribution.

at a distance k^2/l_1 aft of the c.g. position. The c.g. therefore remains in the correct position, as, taking moments about the c.g. of the two concentrated weights,

$$\text{Moment} = W\left(\frac{k^2}{k^2 + l_1^2}\right) l_1 - W\left(\frac{l_1^2}{k^2 + l_1^2}\right)\frac{k^2}{l_1} = W\left(\frac{k^2 l_1 - k^2 l_1}{k^2 + l_1^2}\right) = 0$$

Therefore, the wheel loads in a three-wheel landing are given by Eq. (1).

In a nose wheel first landing, the nose wheel has to stop only the weight, w, immediately over it. The remainder of the weight, $(W - w)$, is free to continue falling until the rear wheels strike the ground. If the airplane is taxiing and the nose wheel strikes a bump, the nose wheel must lift the weight, w, over the bump. The distribution of wheel load by statics would hold only if the rear wheels struck a bump of the same size at the same time as the front wheels. As a further example of the lack of relationship between the nose wheel load from static distribution with that under dynamic conditions, move the rear wheels forward to a position directly under the c.g. The load on the nose wheel by Eq. (1) is now zero. Yet, if the airplane strikes on the nose wheel first, the wheel must still decelerate the weight, w, and the nose wheel load will be determined by Eq. (7). Similarly, if the airplane were to taxi in this condition, the nose wheel would have to lift the weight, w, over the bumps. Thus, design criteria based on static load distribution may give no indication of the true load on the nose wheel.

To determine the usual magnitude of the effective weight, w, the radii of gyration of a number of airplanes were plotted against the airplane length, L, in Fig. 2. For single-seater, single-engined airplanes with the engine in the nose, it was found that the radius of gyration is very nearly 0.184 times the length, or

$$k = 0.184L \tag{10}$$

Substituting in Eq. (8)

$$w = W\left[\frac{(0.184L)^2}{(0.184L)^2 + l_1^2}\right]$$

or

$$\frac{w}{W} = \frac{0.0348L^2}{0.0348L^2 + l_1^2} = \frac{0.0348}{0.0348 + (l_1/L)^2} \tag{11}$$

Values of w/W are plotted against l_1/L in Fig. 3. For

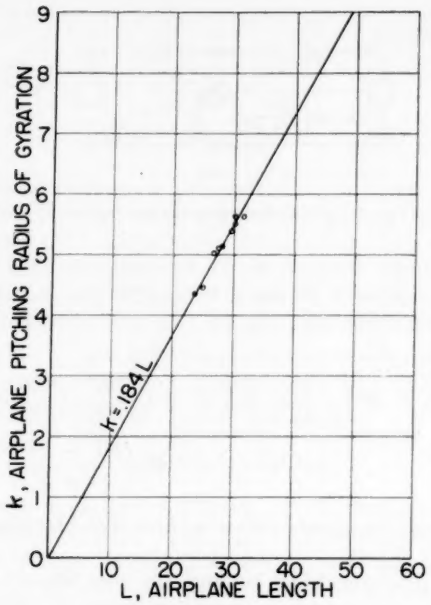

FIG. 2. Variation of pitching radius of gyration with overall length for conventional, single-engined military airplanes.

the usual tricycle gear airplane, l_1 is between 20 and 35 per cent of the airplane length. From Fig. 3 this means that between 46 and 22 per cent of the airplane weight acts on the nose wheel. The static percentage is usually only about 15 per cent, so that the error in designing from the load in the three-wheel attitude may exceed 200 per cent, assuming the same sinking speeds

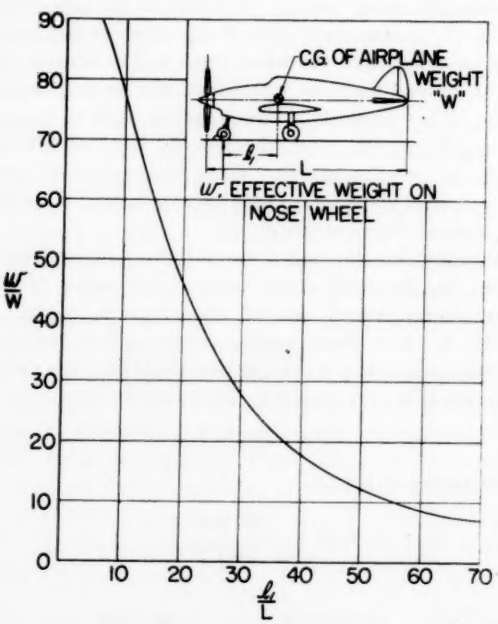

FIG. 3. Variation of percentage airplane weight acting on the nose wheel with percentage overall length of moment arm from nose wheel to center of gravity (for conventional, single-engined military airplanes only).

in both conditions. It should be remembered that these figures apply only to single-engined pursuit airplanes with the engine in the nose. Data on other airplanes indicate that the relationship between the two types of loading varies widely with the airplane type, purpose, loading condition, and size. The ratios between nose first and three-wheel percentages of weight acting on the nose wheel have been found to vary from 4:1 to $1^1/_2$:1.

To relate the single-engined tricycle gear airplane to something more familiar, compare it with the average automobile.[9] Such an airplane, with a wheel base of 35 per cent of its length and with 14 per cent of its weight carried in static position by the nose wheel, bears the same relation to its wheel base as a conventional automobile with a normal 120-in. wheel base would have to a 4-ft. wheel base with the c.g. 7 in. forward of the rear axle. It is easily visualized with this overhanging arrangement how the front wheels would have to lift a large percentage of the car weight in order to pass over a bump.

It is possible from the equations developed to determine the distance, l_1, to give the minimum structural weight. Roughly it may be said that the most efficient position is that where the nose wheel load is the same for the nose first landing as for the three-wheel landing. Assuming the same sinking speed, this could be determined for any particular airplane by setting Eq. (1) equal to Eq. (9) and solving for l_1. However, it has already been stated that the ordinary tricycle gear nose wheel supports about 15 per cent of the airplane weight. Examination of Fig. 3 discloses that for 15 per cent of the weight to be effective on the nose wheel in a nose wheel first landing, l_1 would be nearly 45 per cent of the airplane length. To be consistent with the assumed static distribution, the wheel base would then be $[100/(100 - 15)]45 = 53$ per cent of the length of the airplane. This is obviously too long to be practical. This example, it must be remembered, applies only to conventional, single-engined airplanes and again includes the doubtful assumption that the vertical velocity is the same for both types of landings. If a smaller sinking speed is used in the nose wheel landing or on types with a more compact mass distribution, it may be possible to reach the optimum condition.

It is obvious, however, from Fig. 3, that the nose wheel should be put as far forward as the geometry of the airplane will permit. The increase in load with decrease in l_1 is so rapid as to impose a severe penalty on short-nosed airplanes. Because of this penalty it is usually wise to make the travel of the nose wheel considerably greater than that of the main wheels. If this is done, the acceleration in a nose first landing will be reduced, decreasing the loads on the nose wheel and structure in proportion. The nose wheel and tire should be selected to have a static rating based on the effective weight, w. Consideration should be given

to the ground contact area of the tire chosen. It is desirable that the ground pressure under the effective weight should not be any greater than that of the main tires, otherwise, there will be considerable danger of the tire digging in and burying itself in soft ground with resultant high-bending moments on the nose strut. The fuselage structure must also be designed to take the nose first landing load. This load will usually only be important near the nose wheel, since the high inertia forces of the items in the nose will reduce the loads to be carried aft.

Considering the other two items affected by nose wheel location—the stability against overturning and resistance to porpoising—both are improved by moving the nose wheel forward. The effect on turnover stability can be found under the subject of "Wheel Tread" in this paper (Part 1). The theory of porpoising has been given by Wylie.[3] The subject will also be briefly discussed under the section on "Rear Wheels Location" in this paper (Part 1).

One other item should be mentioned as limiting the nose wheel position in single-engined tractor airplanes—propeller clearance. The nose wheel cannot be placed where strut deflections or tire failure may permit it to enter the propeller disc. Consideration must also be given to providing adequate propeller ground clearance with any possible combination of flat tires.

All the information assembled herein indicates that it is not only desirable but almost essential that the nose wheel be located as far forward as permitted by the geometry of the airplane. The only possible undesirable result of this is propeller interference on single-engined tractor airplanes. All other characteristics will be improved within the practical range of nose wheel positions. The only exceptions to this rule would be airplanes with small pitching radii of gyration, where the nose wheel should be located so as to produce the same load in nose first and three-wheel landings.

Rear Wheel Location

The distance of the main wheels aft of the center of gravity is one of the most important dimensions of a tricycle landing gear because it affects more of the properties than any other single characteristic. The items known to be influenced by the position of the rear wheels are the directional stability, the longitudinal stability, the ability to land with excess air speed and high-sinking speeds without bouncing, the resistance to overturning, the length of take-off run, and the static reaction on the nose wheel. In practice, this dimension is usually confined to a narrow range by two conflicting requirements. If the airplane is to land with excess air speed without bouncing, the wheels must be behind the airplane c.g. when they and the tail buffer are against the ground. Then, in any landing attitude between a tail first and a three-wheel landing, the vertical forces acting at the rear wheels will tend to decrease the angle of attack of the airplane, thus reducing the lift and preventing it from rising into the air again.

Frequently, it is desirable to make take-offs with the nose wheel in the air, thus increasing the percentage of air-borne weight and reducing the wheel drag. To do this satisfactorily the airplane must be stable longitudinally when running on the rear wheels, otherwise, it would either run on all three wheels or on the tail buffer and the rear wheels. To be stable, the condition is that any change in the angle of attack must produce a moment on the airplane tending to restore it to its original attitude. Moments acting on the airplane while taxiing result from the force of gravity, air forces, or wheel friction. Consider first the effect of only the gravity force on the airplane. This might be considered the determination of the stability at zero air speed. Assume the nose wheel lifted off the ground by a down load on the tail of just sufficient magnitude to balance the moment of the airplane about the rear wheels. This down load is best considered as a weight applied to the tail as in Fig. 4 in lieu of the air load

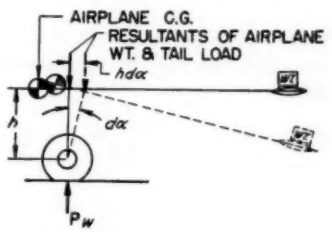

FIG. 4.

that would be obtained by forward velocity. The resultant of the airplane and tail load then passes through the wheel axle and is balanced by the wheel load, P_w. If, however, the angle of attack is increased by a small angle, $d\alpha$, the resultant load moves aft of the wheel axle a distance $hd\alpha$ and produces a moment

$$dM_w = P_w h d\alpha$$

or

$$dM_w/d\alpha = P_w h \qquad (12)$$

This change in moment tends to increase the angle of attack still further. Therefore, the gravity force is destabilizing or the airplane is unstable in this condition at zero air speed.

Next, consider the airplane running, balanced on its rear wheels only as shown in Fig. 5, at an air speed,

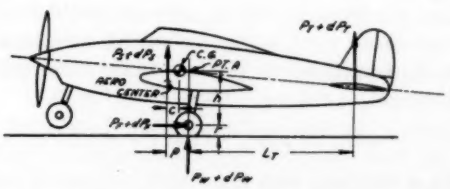

FIG. 5. Conditions when taxiing on the rear wheels.

V, sufficient to produce a dynamic pressure, q. It is assumed that the wheel friction is equal to the wheel load, P_W, times a friction coefficient, μ; that the thrust is equal to the sum of the wheel friction and aerodynamic drag; and that the thrust and aerodynamic drag produce negligible net moments about the c.g. The rate of change of wing-lift coefficient with airplane angle of attack, $dC_L/d\alpha$, includes the ground effect; the rate of change of tail lift coefficient with airplane angle of attack, $dC_{LT}/d\alpha$, includes the effect of wing down-wash and ground effect.

A change in angle of attack, $d\alpha$, will produce a change in lift on the wing (wing area = S)

$$dP_S = Sq(dC_L/d\alpha)d\alpha$$

or

$$dP_S/d\alpha = SqdC_L/d\alpha \tag{13}$$

Similarly, there will be a change in lift on the tail (tail area = S_T)

$$dP_T = S_Tq(dC_{LT}/d\alpha)d\alpha$$

or

$$dP_T/d\alpha = S_TqdC_{LT}/d\alpha$$

These two increases in the lift on the airplane reduce the load on the wheels by an amount $dP_W = -(dP_S + dP_T)$.

$$\frac{dP_W}{d\alpha} = -\frac{dP_S}{d\alpha} - \frac{dP_T}{d\alpha} = -q\left(S\frac{dC_L}{d\alpha} + S_T\frac{dC_{LT}}{d\alpha}\right) \tag{14}$$

The friction on the wheel is reduced also by an amount $dF_W = \mu dP_W = -\mu(dP_S + dP_T)$ or

$$\frac{dF_W}{d\alpha} = -\mu q\left(S\frac{dC_L}{d\alpha} + S_T\frac{dC_{LT}}{d\alpha}\right) \tag{15}$$

The change in moment on the airplane resulting from the air loads only can now be found by taking moments about any convenient point. The point usually used for checking the stability in flight is the c.g. so that will be used here. Accordingly, the change in moment due to air loads is (Fig. 5)

$$dM_A = cdP_S - (p - c)dP_W - (L_T + p - c)\times dP_T - hdP_F$$

Substituting $-(dP_S + dP_T)$ for dP_W

$$dM_A = cdP_S + (p - c)(dP_S + dP_T) - (L_T + p - c)\times dP_T - hdP_F$$

This reduces to

$$dM_A = pdP_S - L_TdP_T - hdP_F \tag{16}$$

This equation, it will be noticed, could have been derived much more easily by taking moments about point A, directly above the rear wheel axles and at the same height as the c.g. Thus, from Fig. 5,

$$dM_A = pdP_S - L_TdP_T - hdP_F$$

which is identical with Eq. (16).

This illustrates an important difference between the stability in free flight and the stability when running on the rear wheels. In free flight any external moment causes the airplane to rotate about the c.g. The condition for stability is therefore that the change in air force moments about the c.g. for a change in angle of attack should tend to restore the airplane to its original attitude. When taxiing on the rear wheels, an external moment tends to rotate the airplane about the point A, since, for small angles, the wheels prevent A from moving vertically while the airplane inertia restrains it fore and aft. It is generally accepted that moving the c.g. aft decreases the stability of an airplane in free flight. This may be stated that as the center of rotation moves aft the stability of the airplane decreases and may even become negative. Therefore, when taxiing on the rear wheels, the stability is similar to what it would be in free flight with the c.g. moved back even with the rear wheel axles. As the rear wheels are always aft of the c.g., the stability is less when taxiing than in flight, and it is easily possible that an airplane that is stable in flight may be unstable in the rear wheel taxiing condition.

The total change in moment on the airplane for a change in angle of attack, $d\alpha$, can now be found by adding Eqs. (12) and (16), thus combining the moments due to gravity forces with those due to air forces.

$$dM_W + dM_A = dM = P_Whd\alpha + pdP_S - L_TdP_T - hdP_F$$

or

$$\frac{dM}{d\alpha} = P_Wh + p\frac{dP_S}{d\alpha} - L_T\frac{dP_T}{d\alpha} - h\frac{dP_F}{d\alpha} \tag{17}$$

Substituting Eqs. (13), (14), and (15) in Eq. (17)

$$\frac{dM}{d\alpha} = P_Wh + q\left[pS\frac{dC_L}{d\alpha} - L_TS_T\frac{dC_{LT}}{d\alpha} + \mu h\left(S\frac{dC_L}{d\alpha} + S_T\frac{dC_{LT}}{d\alpha}\right)\right] \tag{18}$$

For the airplane to be stable, $dM/d\alpha$ must be negative—that is, an increase in angle of attack must produce a negative moment that will tend to return the airplane to its original attitude. An examination of Eq. (18) shows that the first term, P_wh (the load on the wheels times the height, h), is always positive, so that for stability the term in the brackets must be negative. If this term is negative, then the stability improves with q or in proportion to the velocity squared. At low air speeds, the airplane is always unstable for the condition of running only on the rear wheels. This is not important, however, as at low air speeds there is not enough tail load available to lift the nose wheel off the ground.

In practice, it is usually satisfactory if the airplane becomes stable before it reaches the take-off speed. As the airplane approaches the take-off speed, the load on the wheels, P_w, becomes smaller and smaller, so

that at the instant of take-off the term $P_w h$ in Eq. (18) becomes zero. Therefore, to be stable at take-off the condition is that the term in the brackets must be equal to, or less than, zero.

$$p\frac{SdC_L}{d\alpha} - L_T S_T \frac{dC_{LT}}{d\alpha} + \mu h\left(S\frac{dC_L}{d\alpha} + S_T\frac{dC_{LT}}{d\alpha}\right) \leqq 0$$

or

$$L_T S_T \frac{dC_{LT}}{d\alpha} \geqq pS\frac{dC_L}{d\alpha} + \mu h\left(S\frac{dC_L}{d\alpha} + S_T\frac{dC_{LT}}{d\alpha}\right) \quad (19)$$

If Eq. (19) is not satisfied, the airplane will become progressively less stable as the speed increases. This would necessitate the pilot holding the nose wheel on the ground until take-off speed was reached, at which any slight disturbance would produce a sudden increase in the angle of attack, causing the airplane to leap into the air. If sufficiently unstable, it might be impossible for the pilot to hold the nose on the ground until take-off speed was reached. Should the pilot attempt a nose high take-off with an unstable airplane, the angle of attack would increase until the wing stalled. Beyond the stall, the slope of the wing-lift curve becomes negative so that the terms involving $dC_L/d\alpha$ become negative, the equation is satisfied, and the airplane becomes stable again. In practice, the tail buffer usually strikes the ground and drags before the stall is passed sufficiently to reverse the lift curve slope. The airplane may then run along on the rear wheels and tail buffer or, if sufficiently unstable, the angle of attack may increase still further, leaving only the tail buffer on the ground. In either case, the take-off run would be increased by the high drag of the stalled wing plus that of the tail buffer, and the airplane would be forced off the ground in a stalled attitude. For the case of take-off on the tail buffer alone (which can occur only on airplanes where the buffer is quite well forward), the airplane would become laterally unstable as soon as the rear wheels left the ground and would be very likely to go up on one wing tip. Thus, it can be seen that while a tricycle gear airplane so constructed as to be unstable with the nose wheel in the air could be flown it would be a highly treacherous and unsatisfactory arrangement.

Eq. (19) is not in a form that is easily used, since it involves the rates of change of lift coefficients with airplane angle of attack. As these are usually unknown, the formula will be transformed into a form using the lift curve slopes of the airfoils for infinite aspect ratio.

Let

a = slope of wing-lift curve = $dC_L/d\alpha$ for infinite aspect ratio
a_T = slope of tail lift curve = $dC_{LT}/d\alpha$ for infinite aspect ratio
R = wing aspect ratio
R_T = tail aspect ratio

The slope of the lift curve of a wing of aspect ratio, R, in terms of the slope for infinite aspect ratio is[1]

$$dC_L/d\alpha = a/\{1 + [a(1 - \sigma)/\pi R]\} \quad (20)$$

where σ is a factor depending on the ratio of wing height above the ground to wing span and is available in standard texts on aerodynamics.

The tail operates in the down-wash of the wing. The change in the tail angle of attack for a given change in airplane angle of attack is smaller by the change in the down-wash angle, $d\beta$. Or

$$d\alpha_{Tail} = d\alpha_{Airplane} - d\beta \quad (21)$$

When the ground effect is considered, $d\beta/d\alpha$ at the tail varies with its height above the ground. If the tail is approximately even with, or above, the wings[1]

$$d\beta/d\alpha = (2a/\pi R)(1 - \sigma) \quad (22)$$

Accordingly, using Eqs. (20), (21), and (22), the rate of change of tail-lift coefficient for airplane angle of attack becomes:

$$\frac{dC_{LT}}{d\alpha} = \left[\frac{a_T}{1 + (a_T/\pi R_T)(1 - \sigma_T)}\right]\left[1 - \frac{2a}{\pi R}(1 - \sigma)\right] \quad (23)$$

where σ_T is the ground effect factor for the tail.

Eq. (19) may now be rewritten, using Eqs. (20) and (22), as

$$\eta(L_T - \mu h)\frac{S_T a_T}{Sa}\frac{[1 + (a/\pi R)(1 - \sigma)]}{[1 + (a_T/\pi R_T)(1 - \sigma_T)]} \times \left[1 - \frac{2a(1 - \sigma)}{\pi R}\right] \geqq p + \mu h \quad (24)$$

where η is a tail efficiency factor to account for interference effects.

The stability of the airplane may be determined by Eq. (24), since all of the quantities are known except η, which may either be determined from wind-tunnel tests or estimated from experience. However, for conventional airplanes this equation may be simplified considerably by making a few slightly conservative assumptions. The wing height above the ground is usually between one-tenth and two-tenths of the wing span. Within this range[1] σ has values between 0.655 and 0.485. The effect of σ on the final result is small, and it will usually be slightly conservative to assume σ equal to 0.5. The height of the tail surface above the ground varies with the angle of attack of the airplane, but in level position the tail is usually about one-half its span above the ground. For this attitude σ_T may be assumed zero with only a small conservative error.

As the attitude of the airplane changes, moving the tail closer to the ground, σ_T will increase, thus improving the stability. The maximum possible improvement, if the tail were just above the ground line,

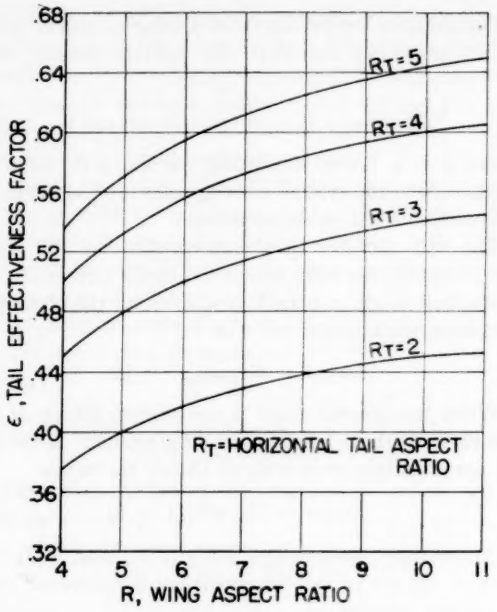

FIG. 6. Tail effectiveness factor as a function of wing and horizontal tail aspect ratios.

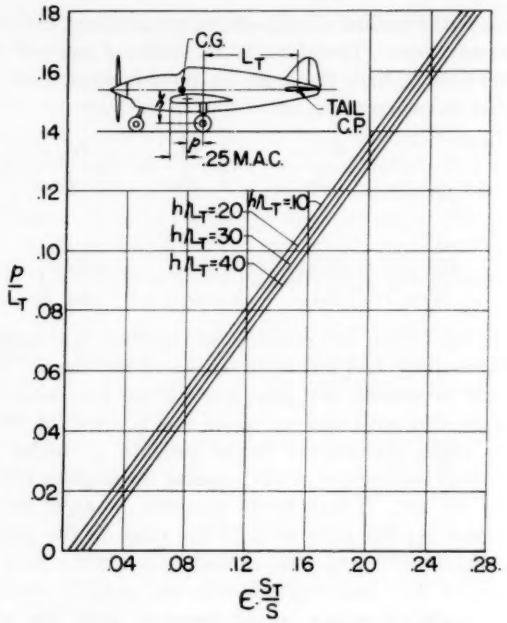

FIG. 7. Graph for determination of static longitudinal stability when taxiing on the rear wheels.

would be $200/R_T$ per cent, which, for usual tail aspect ratios of about four, would be not more than 50 per cent. In most cases, $\sigma_T = 0$ will be a satisfactory approximation for the most severe condition with the tail at maximum height. The slope of the lift curves of both the wing and tail for infinite aspect ratio may be assumed to be equal—a condition that is very nearly true for modern airfoils. In addition, they may be set equal to the theoretic value of 2π. This value is slightly higher than usually realized, but it can be seen from Eq. (24) that the actual numerical value is of secondary importance so long as the correct ratio is kept between the values for the wing and tail. Two other items—μ, the coefficient of friction, and η, the tail efficiency—can be replaced by constants. The coefficient of rolling friction[2] on airports in fair condition is about 0.03.

Tail efficiencies on modern airplanes are usually 70 to 80 per cent; so for preliminary design around work a value of 0.7 should be satisfactory. Substitution of these terms in Eq. (24) gives:

$$0.7\frac{S_T}{S}(L_T - 0.03h)\frac{[1 + (2\pi/\pi R)(1 - 0.5)]}{[1 + (2\pi/\pi R_T)(1 - 0)]} \times \left[1 - \frac{4\pi(1 - 0.5)}{\pi R}\right] \geqq p + 0.03h$$

This reduces to

$$0.7\frac{S_T}{S}(L_T - 0.03h)\frac{R_T(R - 1)}{R(R_T + 2)} - 0.03h \geqq p \quad (25)$$

The term $(L_T - 0.03h)$ is the effective tail arm. The second part of this term is small compared to L_T and can be ignored.

Also, if a tail effectiveness factor, ϵ, is substituted for $R_T(R - 1)/R(R_T + 2)$, Eq. (25) becomes

$$(0.7\epsilon S_T/S) - (0.03h/L_T) \geqq p/L_T \quad (26)$$

In Fig. 6, values of ϵ are plotted against wing aspect ratio, R, for constant values of tail aspect ratio, R_T. Fig. 7 has values of p/L_T plotted against $\epsilon S_T/S$ for constant values of h/L_T. The entire solution for the maximum value of p may thus be done graphically if only the wing aspect ratio and area, tail aspect ratio and area, tail length, and c.g. height are known. The answer as finally determined should be satisfactory for design work in conventional airplanes. If the airplane lies outside the range of assumptions, the stability should be determined directly from Eq. (24). It should be remembered in applying this equation that the distances p and L_T are always measured parallel to the ground line, while h is measured perpendicular to it, regardless of the attitude of the airplane. In practice, L_T and h are little affected by angle of attack, but p usually decreases rapidly as the angle of attack increases. Therefore, as the angle of attack is increased, the stability improves.

By making the same substitutions and approximations in Eq. (18) as were made on Eq. (19) and by replacing the wheel load, P_w, by the airplane weight less the wing lift, or $(W - qSC_L)$, the dynamic pressure, q, and consequently the speed at which the airplane becomes stable may be calculated for any particular angle of attack.

$$q = \frac{Wh}{2\pi\eta L_T S_T \left[\frac{R_T(R-2)}{R(R_T+2)}\right]} \times \frac{1}{-2\pi S(p+\mu h)\frac{R}{R+1} + C_L Sh} \quad (27)$$

In using this equation, the values of p and C_L must be for the same angle of attack and the ground effect must be considered in determining C_L.

The minimum speed at which the elevators and wing can lift the nose wheel into the air may be determined if the lift coefficient of the tail is known for the elevator full-up position and airplane level angle of attack. At speeds lower than the minimum at which enough down load on the tail can be developed to lift the nose wheel into the air, the stability when running on the rear wheels only has no real meaning unless it is desired to consider the extreme case when the nose wheel strikes an obstruction large enough to throw it into the air. It would be desirable to have the airplane stable at all possible angles of attack at this minimum speed, but this condition usually cannot be realized. The next best thing would be to have the airplane stable at this minimum speed and the angle of attack corresponding to the attitude with the tail buffer just above the ground. Attainment of this condition may also be impossible, since any changes made to improve the stability, such as reducing p or increasing the tail arm or area, will reduce the speed at which the nose wheel can be lifted and thereby require a further stability increase.

Little information is available on the degree of stability actually used on tricycle gear airplanes. Approximate checks on several airplanes indicate minimum stable speeds of the order of two-thirds to nine-tenths of the take-off speed. This apparently is not usually the result of design for stability but rather is the result of a desire to make it as easy as possible for the pilot to lift the nose into the air and to reduce the static nose wheel load.

At present, it is felt that Eq. (26) provides the best criterion of stability. If this equation is satisfied for the level attitude of the airplane, the stable speed will be reached before the take-off speed and appreciably so at the higher angles of attack. No dangerous conditions should arise from instability below the take-off speed, the worst possibility being a banging and dragging of the tail buffer on the ground and a consequent increase in length of take-off run.

The analytic treatment of the stability problem given herein is a modification of the method of Wylie[3] with the addition that the effect of c.g. height is considered. As given here, the criterion developed is a measure of the static stability only. It may be applied to the dynamic case if desired, but it is felt that there is little to be gained by such a procedure.

The two conditions—(1) that the c.g. must be forward of the rear wheels at the maximum ground angle and (2) that the airplane must be stable on the rear wheels at take-off speed—usually limit the satisfactory rear wheel location to a narrow range. The effect of changing the wheel location within this region on other characteristics of the airplane will next be considered.

The directional stability is proportional to the distance of the rear wheels aft of the c.g. The relationship between this distance and the directional stability is developed in the section of this paper on "Wheel Tread" (Part 1), where it is found that the minimum acceptable distance from the wheels to the c.g. usually gives more than adequate directional stability.

The resistance to porpoising or longitudinal oscillation when running on all three wheels increases with rear wheel distance from the c.g. This type of oscillation usually only occurs with extremely short wheel bases and high c.g. positions. Generally, it appears only at low speeds, since the damping effect of the tail prevents oscillation at high speeds. The only detrimental effect, therefore, is possible discomfort of the crew. This condition is not considered important enough to warrant further discussion. However, if desired, the approximate period of oscillation may be calculated by the method outlined by Wylie.[3]

Resistance to overturning is improved by keeping the rear wheels close to the c.g. The effect is usually small, the most important factors in preventing overturning being the tread and distance from c.g. to nose wheel. This problem is considered in the section of this paper on "Wheel Tread" (Part 1).

From the previous considerations, the best position for the rear wheels is believed to be just aft of the rearmost c.g. with the tail buffer on the ground. Placing the wheels further aft of the c.g. can only improve the porpoising characteristics, which are unimportant, and the directional stability, which is usually adequate and may thus become excessive. At the same time, the longitudinal stability during nose-high take-offs and the resistance to overturning will be decreased. Thus there is one partially desirable effect against two and possibly three undesirable effects. Therefore, except in the case when it is necessary to improve the porpoising characteristics at the expense of the other items, the rear wheels should be located as far forward as permitted by the rearmost c.g.

Wheel Tread

General

The wheel tread is a dimension that, in single-engined types, is not usually limited or closely controlled by the airplane geometry. In addition, the characteristics of a tricycle gear airplane affected by the tread are also a function of wheel base and fore-and-aft location of the c.g. The determination of the wheel positions fore and aft has been discussed in the section of this paper on

"Wheel Base" (Part 1), where it is found that several of the airplane characteristics determine the longitudinal wheel locations within narrow limits and that these characteristics are independent of the tread. Therefore, in the design of a tricycle landing gear, the fore-and-aft wheel positions should first be determined by the aforementioned criteria. The wheel tread can then be adjusted to make satisfactory the properties of the landing gear affected by both wheel base and tread. In multiengined airplanes where the tread is determined by the nacelle spacing, it may be necessary to modify this method. The usual nacelle spacing, however, is sufficient to give an entirely adequate tread.

The qualities influenced by the wheel tread are the resistance to overturning and the ease of steering by differential braking. In addition, there may be secondary effects on the directional stability.

Stability Against Overturning

An airplane may be said to be stable against overturning if the wheels will slide before they can develop a frictional force sufficient to upset the airplane. Consider the triangle formed by the three wheels as shown in Fig. 8. Let the resultant inertia and gravity force acting at the c.g. be represented by a vector. If this resultant vector intersects the ground inside the triangle, then the airplane will not overturn; if it intersects the ground outside the triangle, then it will overturn.

If

b = tread
P_w = total wheel load (all three wheels)
h_1 = height of c.g. above ground line

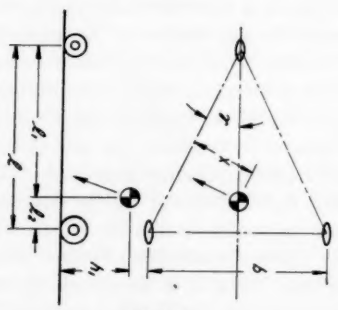

FIG. 8.

The largest possible magnitude of the horizontal component of the force acting on the airplane cannot exceed μP_w, the maximum frictional force of the wheels. Obviously, this force is most likely to upset the airplane when it acts in a direction perpendicular to one side of the triangle. The overturning moment is then:

$$M_0 = \mu P_w h_1 \tag{28}$$

The stabilizing or resisting moment is

$$M_s = P_w X \tag{29}$$

If the airplane is not to overturn, $M_s \geqq M_0$, or

$$P_w X \geqq \mu P_w h_1 \text{ or } X \geqq \mu h \tag{30}$$

But

$$X = l_1 \sin \gamma \text{ and } \sin \gamma = \frac{b/2}{\sqrt{l^2 + (b/2)^2}}$$

So that

$$X = l_1 b/2\sqrt{l^2 + (b/2)^2} \tag{31}$$

Substituting Eq. (31) in Eq. (30) and solving for b

$$b \geqq 2\mu h_1 l/\sqrt{l_1^2 - \mu^2 h_1^2} \tag{32}$$

And

$$b/l = 2\mu h_1/l\sqrt{(l_1/l)^2 - \mu^2(h_1/l)^2} \tag{33}$$

Minimum values of tread to prevent overturning can be calculated from Eq. (32) if the coefficient of friction, μ, is known. Eq. (33) is the nondimensional form of Eq. (32), expressing the minimum satisfactory ratio of tread to wheel base in terms of the ratios of c.g. height to wheel base and nose wheel arm (l_1) to wheel base.

The coefficient of friction, μ, varies with the type of surface and its condition. A value of 0.55 is customarily used in brake design to produce a brake capable of skidding the tire. A coefficient of friction of 1.00 is usually assumed in ground-loop conditions for design of landing gears. These conditions, however, are usually specified so as to give certain loads on the structure and not necessarily to simulate actual conditions. In view of these wide discrepancies between the values for the coefficient of friction, no final criteria can be given. A coefficient of 0.85, however, is believed to be adequate for use in this formula. This has a slightly better than 1.5 safety factor over 0.55, the coefficient used for braked friction.

Objections have been raised to this overturning criterion on the ground that so long as the nose wheel is free swiveling the airplane will turn sufficiently in the direction it was yawed to prevent overturning. To turn, however, the rotational inertia of the airplane must be overcome. Accordingly, computations were made of the lateral acceleration of airplanes landing with various angles of yaw by assuming the side load resisted only at the rear wheels. It was found that angles of yaw above approximately 10 deg. would be sufficient to cause the rear wheels to skid. The resisting frictional force would, of course, be proportional to the vertical load on the rear wheels rather than on all three wheels. Since the rear wheels usually support about 85 per cent of the airplane weight, the force necessary to slide the wheels is about 85 per cent of what it would be to slide all three wheels. However, as mentioned previously, the maximum value of the coefficient of friction is about 1.00. Using 0.85 as was done in computing the curves, will, therefore, approximately compensate for the swiveling of the nose wheel.

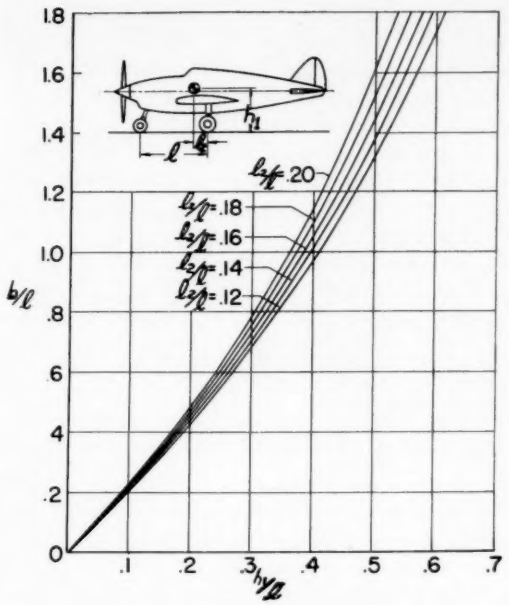

FIG. 9. Minimum ratio of tread to wheel base which will prevent overturning for a coefficient of friction of 0.85.

Values of b/l have been plotted against h_1/l for constant values of l_2/l in Fig. 9, using $\mu = 0.85$. These curves may be used for other values of μ by multiplying the values of h_1/l by $\mu/0.85$ and getting an equivalent h_1/l. Read the value of b/l from the curves using the equivalent value of h_1/l.

The curves are labeled in terms of l_2/l, where $l_2 = (l - l_1)$, instead of l_1/l as indicated by the formula, since l_2/l corresponds to the percentage of static load on the nose wheel and is usually more convenient than l_1/l.

Directional Stability and Ease of Steering

The directional stability is determined by the distance of the rear wheels aft of the c.g. and the height of the c.g. above the ground line. Neither of these dimensions is related to the tread. Ease of steering may be said, however, to be inversely proportional to the directional stability and, if the steering is done by differential braking, directly proportional to the tread. It is difficult to give a criterion for directional stability alone because, since all tricycle landing gears are directionally stable so long as the rear wheels are behind the c.g., the problem becomes one of the degree of directional stability desired. It has been pointed out in the section of this paper on wheel base (Part 1) that the value of l_2 is usually controlled by requirements distinct from those of directional stability. Similarly, h_1 is usually determined by the airplane geometry and cannot be altered to adjust the directional characteristics. The directional stability is, therefore, usually set by other requirements of the airplane, and this degree of stability must be accepted as a characteristic of the airplane. This is not so serious as it might at first seem, since airplanes can be operated satisfactorily over a wide range of directional characteristics. The conventional landing gear is unstable until the air speed becomes sufficient for the stabilizing characteristics of the tail to overcome the instability of the landing gear. Yet little difficulty is experienced by pilots in overcoming ground-looping tendencies except in airplanes with extremely narrow treads, where the wheel brakes cannot supply an adequate stabilizing moment, or under other adverse conditions. As the tricycle landing gear is always stable, ground looping cannot occur, and it is never necessary for the pilot to supply a stabilizing moment. Instead, the problem is reversed; in order to make a turn the pilot must provide a moment to partially overcome the naturally stable characteristics of the airplane. Accordingly, the sharpness of turn depends on the magnitude of the turning moment that can be applied which, assuming the turning is done by differential braking, depends on the wheel tread and tire coefficient of friction.

Consider a tricycle gear airplane of mass, W/g, following a path of radius of curvature, R, at a velocity, V, as shown in Fig. 10. There will be a centrifugal force acting outward at the c.g. of

$$F = (W/g)V^2/R \tag{34}$$

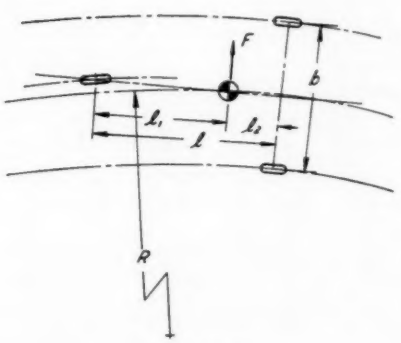

FIG. 10.

The nose wheel is free to swivel and, therefore, cannot resist any of the side force, F, which accordingly must be taken entirely by the rear wheels. This produces a moment tending to return the airplane to a straight path, of

$$M_1 = l_2F = l_2WV^2/gR \tag{35}$$

The force, F, also acts at a height, h_1, above the ground line, thereby producing a moment tending to increase the load on the outside wheel and reduce it on the inside. The change in load is (using Eq. (34))

$$\Delta P = Fh_1/b = h_1WV^2/bgR \tag{36}$$

This change in load will increase the wheel friction on the outside of the turn and, accordingly, produce

another moment tending to restore the airplane to a straight course. The reduction of load on the inside of the turn will also have the same effect. The airplane, following the path of radius, R, therefore has a total moment tending to restore it to a straight course equal to Eq. (35) plus Eq. (36), which reduces to

$$M_s = (WV^2/gR)(l_2 + \mu h_1) \tag{37}$$

If steering is done by differential braking, the moment produced by braking the inside wheel is

$$M_B = (b/2)(\mu_B - \mu_0)P_I \tag{38}$$

where μ_B is the coefficient of friction of the braked wheel as distinguished from μ_0, the coefficient of friction of the unbraked wheel, and P_I is the load on the inside wheel. But P_I is equal to the static load on the wheel less ΔP.

$$P_I = [(W/2)l_1/l] - [h_1WV^2/bgR] \tag{39}$$

So that substituting Eq. (39) in Eq. (38)

$$M_B = (b/2)(\mu_B - \mu_0)W[l_1/2l - (h_1V^2/bgR)] \tag{40}$$

To make a steady turn, M_B must equal M_S, or using Eq. (37) and Eq. (40)

$$(WV^2/gR)(l_2 + \mu_0 h_1) = (b/2)(\mu_B - \mu_0) \times W[l_1/2l - (h_1V^2/bgR)]$$

Solving for R

$$R = [4V^2l/gbl_1]\left[\frac{l_2 + {}^1/_2 h_1(\mu_B + \mu_0)}{\mu_B - \mu_0}\right] \tag{41}$$

The value of R may now be determined by substituting numerical values in Eq. (40). The sharpest turn will, of course, be made by sliding the inside wheel. For this case μ_B will be assumed to be equal to 0.55 and μ_0 to 0.03. The equation then becomes

$$R = 0.514\,\frac{V^2}{b}\,\frac{l}{l_1}\,(l_2 + 0.29h_1) \tag{42}$$

where V is in m.p.h. and the rest of the dimensions are in ft.

As an example, consider a typical pursuit airplane, with the following dimensions, taxiing at 30 m.p.h.—$b = 8.33$ ft., $l = 10$ ft., $l_1 = 8.75$ ft., $l_2 = 1.25$ ft. and $h_1 = 5.0$ ft. Then $R = 172$ ft.

Thus, in this case, the airplane is so stable directionally that at 30 m.p.h. with one main wheel locked it takes a 350-ft. circle to turn around. The diameter of this circle is proportional to the square of the speed so that the size for any other speed can be found by a simple ratio. At a stalling speed of approximately 80 m.p.h., the diameter would be nearly 2,500 ft. Thus, no serious consequences would result from locking one wheel, even when landing, since the turning radius is so large. It is impossible to tip a tricycle gear airplane up on one wing by differential braking because, as the radius of turn becomes smaller, the load on the inside tire which is providing the turning moment decreases, thus reducing the frictional force and the turning moment. For the airplane to go up on one wing, the inside wheel would have to lift clear of the ground, reducing its turning moment to zero. The frictional drag of the wheel on the other side would then produce a turning moment in the opposite direction which would result in a centrifugal force, forcing the braked wheel back onto the ground. It is possible, however, by increasing the tread, b, sufficiently to make R so small that the centrifugal force is greater than the resistance of the tires to sliding sidewise. That is, if μ_s is the coefficient of friction for sliding sidewise,

$$(W/g)V^2/R \geqq \mu_s W l_1/l$$

Or, to prevent sliding

$$R \geqq V^2l/\mu_s g l_1 \tag{43}$$

If μ_s is taken to equal 0.55, the airplane of the example would begin to skid at 30 m.p.h. for a radius of turn of 125 ft. Thus, no matter what the tread was increased to, the airplane could not turn around in a circle less than 250 ft. in diameter at 30 m.p.h. Since the turning radius is inversely proportional to the tread, the corresponding value of tread required would be $b = 172/125 \times 8.33 = 13.75$ ft. The same result could have been obtained by setting Eq. (43) equal to Eq. (41) and solving for b.

In applying these equations, it should be remembered that, in their development, R was considered large in relation to the tread. It can be seen from Fig. 10 that for small values of R the frictional drag of the nose wheel would have a stabilizing effect and the centrifugal force, F, would not be perpendicular to the planes of the rear wheels. For radii greater than five times the tread, these discrepancies have a negligible effect.

References

[1] Stalker, E. A., *Principles of Flight*, The Ronald Press Company, New York, 1931.

[2] Wetmore, J. W., *The Rolling Friction of Several Airplane Wheels and Tires*, N.A.C.A. T.R. No. 583, Washington, D.C., 1937.

[3] Wylie, Jean, *Dynamic Problems of the Tricycle Alighting Gear*, Journal of the Aeronautical Sciences, Vol. 7, No. 2, pp. 56–67, December, 1939.

[4] Kantrowitz, A., *Stability of Castering Wheels for Aircraft Landing Gears*, N.A.C.A. T.R. No. 686, Washington, D.C., 1940.

[5] Taylor, J. Lockwood, *Oscillation of Castering Wheels*, Aircraft Engineering, Vol. 13, No. 143, p. 13, January, 1941.

[6] Warner, E. R., *The Double Spindle Wheel Castering System for Airplane Nose Wheels*, Cleveland Pneumatic Tool Company, Cleveland, O.

[7] Howard, Walter B., *A Full Scale Investigation of the Effect of Several Factors on the Shimmy of Castering Wheels*, N.A.C.A. T.N. No. 760, Washington, D.C., 1940.

[8] Wernitz, W., *Tricycle Undercarriage Development*, Aircraft Engineering, Vol. 13, No. 143, pp. 6–12, January, 1941; translated from Luftwissen, Vol. 7, No. 3, March, 1941.

[9] Schilling, R., and Fuchs, H. O., *Modern Passenger-Car Ride Characteristics*, Journal of Applied Mechanics, Vol. 8, No. 2, pp. A-59–A-66, June, 1941.